Survey of porewater geochemistry within
deep marine hydrocarbon seep sediments of the Scotian Slope, Canada

By
Nikita Lakhanpal

A Thesis Submitted to
Saint Mary's University, Halifax Nova Scotia
In Partial Fulfilment of the Requirements for
the Degree of Bachelor of Science with Honours in Geology.

May 2022, Halifax, Nova Scotia.

Approved: Dr. G. Todd Ventura
Supervisor

Approved: Dr. Venus Baghalabadi
Supervisor

Approved: Dr. Marc Lamoureux
External Reviewer

Date: 27th May 2022

Table of Contents

List of Figures....4
List of Tables....5
Acknowledgements....6
Abstract....7
1. Introduction....8
1.1 Scotian Slope....8
1.1.1 Geological History and Setting....8
1.2 Hydrocarbon Seep Sites....10
1.3 Biogeochemical Cycles....12
1.3.1 Nitrogen Cycle....12
1.3.2 Sulfur Cycle....13
1.3.3 Carbon Cycle....13
1.4 Redox Gradients....14
1.5 Porewater (PW)....15
1.6 Ion Chromatography (IC)....16
1.7 Standard Addition Method....17
1.8 Calibration Curve Method....18
1.9 Research Objective and Hypothesis Statement....18
2. Experimental....19
2.1 Instrument and Sample Preparation Equipment....19
2.2 Reagents and Chemicals....20
3. Methodology....20
3.1 Preparation of Mobile Phase....20
3.2 Preparation of Standard....21
3.3 Ion Chromatographic Analysis....21
3.4 Sediment Porewater....22
3.5 Standard Addition Methodology....22
3.6 Calibration Curve Methodology....24
3.7 Data Analysis....24
4. Results and Discussion....25

4.1 Comparative study of standard addition and calibration curve methods.....35
4.2 Porewater concentration as a function of ocean floor surface sediment depth.....38
4.2.1 Scotian Slope core survey.....38
4.2.2 Site specific study.....41
4.2.2.1 Outside the Seep.....42
4.2.2.2 Inside the Seep.....43
4.3 Comparative study of ambient marine benthic sediments to hydrocarbon impacted Sediments.....47
4.3.1 Nitrate and Nitrite Recycling.....47
4.3.2 Sulfate Reduction.....49
4.3.3 Carbonate Variation.....50
5. Conclusions.....51
6. Appendix.....52
6.1 Appendix A.....52
6.2 Appendix B.....57
7. List of References.....60

List of Figures

Figure 1. Geographical extent of the Scotian Shelf and the Scotian Slope (ocean depth increases from a lighter blue to a darker blue). Arrows represent rough extent of the divided zones of the Scotian Margin. (modified from Government of Canada, 2018). 10

Figure 2. Diagram showing an idealized electron tower redox reaction succession in marine conditions and how the ion chemistry changes with increasing depth. Red arrows point toward elements of interest for this study. (modified from Jilbert, 2016). 15

Figure 3. Flow diagram showing instrumental components of an IC (modified from Nesterenko & Paull, 2017). 17

Figure 4. Geological setting of the Scotian Slope and the location of all the collected cores. Sites of interest for this study are circled in red. .....……...26

Figure 5 (a-e). Comparison of standard addition (blue) versus calibration curve (black) data for different anion concentrations. .....……38

Figure 6 (a-e). Different anion concentrations (ppm) versus depth (cm). Red circles are representative of the outliers. Two of the red circles in the nitrite concentration figure are representing core 49 (hydrocarbon positive site) and core 13 (hydrocarbon negative site). The red circles represent the outliers for each anion concentrations and which core they belong to.....41

Figure 7 (a-d). Depth profiles of anions detected across various cores. Note the varying concentration scale for each core. 46

Figure 8 (a-e). Different anion concentrations (ppm) v/s depth (cmbsf) divided for hydrocarbon positive cores (green) v/s hydrocarbon negative cores (black). 51

List of Tables

Table 1: Amount of PW, Standard Mix and HPLC grade water mixed to obtain each injection for the initial set of samples.....23

Table 2: Amount of PW, Standard Mix and HPLC grade water mixed to obtain each injection for the latter set of samples.....23

Table 3: Regression equations produced for the calibration curve method.....24

Table 4: Geographic location of samples and detected presence of hydrocarbons.....26

Table 5: Standard addition determined anion concentrations.....29

Table 6: Calibration curve determined concentrations.....32

Acknowledgements

I would like to express my deepest and heartfelt gratitude to my supervisors, Dr. G. Todd Ventura and Dr. Venus Baghalabadi for their continuous support and supervision throughout this whole process. Both Todd and Venus have been exceptional mentors and have allowed me to explore my boundaries further than I could ever have imagined. I fall short on words to be able to express how they never let me give up.

I would further like to thank Dr. Marc Lamoureux for providing me with his expertise and knowledge around this subject. I would also like to thank Natasha Morrison and Adam MacDonald at the Nova Scotia Department of Natural Resources and Renewables, Halifax, Canada for their knowledge and proficiency in acquiring the sediment samples and in the process allowing me to learn a lot.

I would also like to acknowledge the continuous help and support from Jeremy Bentley and Anirban Chowdhury from the Organic Geochemistry Lab at SMU. I would also like to thank my family and friends for their support and understanding while I ventured out on this learning curve and to all the faculty members and friends in the Department of Geology at SMU for extending a helping hand whenever needed.

Survey of porewater geochemistry within deep marine hydrocarbon seep sediments of the Scotian Slope, Canada.

Abstract

The ocean floor surface sediments of the Scotian Slope, Nova Scotia are host to a complex network of microbially mediated reactions that knit together the carbon, sulfur, and nitrogen biogeochemical cycles. Limited diffusion between the upper water column and ocean floor muds pore space, coupled with competitive microbial ecological niche partitioning, leads to the formation of biogeochemically controlled redox gradients. The energetics of such gradients are further governed by microbial heterotrophy with the deposition of detrital organic matter that is primarily sourced from terrestrial runoff and upper water column productivity. However, these microbial biogeochemical zones change if surface sediments are impregnated by hydrocarbon seepage that migrates up from deeper within the basin. Porewater profiles of F^-, NO_2^-, NO_3^-, CO_3^{2-} and SO_4^{2-} were used to reconstruct biogeochemical stratification depth profiles that can provide comparative evidence for anion behaviour in active cold seep sites. These profiles define microbial metabolic processes within the sediment subsurface. To test this hypothesis, 50 samples stratigraphically collected across 9 sediment cores were separated, centrifugated and analyzed using ion chromatography. A comparative study between two methods of data analysis was applied to the samples. The internal calibration method of standard addition proved to be a better method than external calibration method of calibration curve to measure porewater anion concentrations of natural samples with complex matrices and a varying range of concentrations. For this reason, porewater anion concentrations were compared using the standard addition method. Fluoride concentration seems uncorrelated to sediment depth and unique sample heterogeneity might be the leading factor to its variation. However, NO_2^-, NO_3^-, and SO_4^{2-} display decreasing concentrations with increasing depths. Carbonate displays a steady variation in concentration possibly attributing to precipitated aggregates of carbonate rocks in the ocean floor surface sediments not being subject to a massive change. Sulfate concentration decreases dramatically in both ambient and hydrocarbon impacted marine benthic sediments although, in hydrocarbon impacted sites, it appears to occur at a much shallower depth suggesting that the redox gradient is much more pronounced and as much sulfate reduction has not yet transpired with the ambient sediments at the same depth. Nitrate and NO_2^- trends also show similar pronounced reduction patterns occurring at shallower depths for hydrocarbon impacted sediments suggesting widespread increased microbial and bacterial activity in these regions.

Date submitted: 27th May 2022

1. Introduction

Cold seep sites can be found in marine settings along active and passive margins. These areas are environments where emissions of H_2S, CH_4, and other hydrocarbon-rich fluid seepage occurs. In the oceanic sediments around these seep sites, there is continuous biodegradation and remineralization of organic matter occurring. The dominant biogeochemical process guiding the geochemistry in cold seep sites is the anaerobic oxidation of methane (AOM) via sulfate reduction (SR) (Joye et al., 2004). For biogeochemical studies, reconstruction of elemental concentration using ion-exchange chromatography in the deep oceanic surface sediments can be a useful tool to study the behavior of organic matter rich sediments that have been impregnated by hydrocarbon seepage. The ocean floor surface sediments of the Scotian Slope, Nova Scotia are host to a complex network of microbially mediated reactions that knit together the carbon, sulfur, and nitrogen biogeochemical cycles. Our knowledge of the deep marine ocean floor surface sediments is limited, but continuously increasing around the controls and transformations of the recycling of biogenic material in these areas (Brunnegård et al., 2004).

1.1. Scotian Slope

1.1.1. Geological History and Setting

The Scotian Slope is a passive margin located off the coast of Nova Scotia. Formed within the Appalachian orogeny during the separation of Africa from North America during the Mesozoic and the breakup of Pangaea (Mosher & Wach, 2009). The area off the coast of Nova Scotia is referred to as the Scotian Margin. Rifting of the Scotia Margin began from 230–175Ma, from the middle Triassic to early Jurassic, followed by seafloor spreading during the Jurassic (Welsink et al., 1989). A combination of deep basin syn-rift deposits overlaying thick successions of salt

deposits, faults, and salt tectonic-based structures make-up the facies of the slope (Mosher & Wach, 2009). The abundant salt structures can produce hydrocarbon traps creating suitable exploration targets (Mosher & Wach, 2009). The thick sediment fill of the slope coupled with the complex structural setting makes it a highly perspective location for hydrocarbon formation. The modern margin is roughly divided into the shelf, slope, and rise. The shelf extends from ~125 – 230 km offshore, while the slope extends from the edge of the shelf to ~2000 m in depth (Government of Canada, 2018). The subsequent depth from 2000 – 5000 m is categorized as the Scotian Rise (Government of Canada, 2018). The shape of the ocean basin influences and guides the biological and geochemical processes. The shelf has been the site of oil and gas production since the late 1960s (Department of Natural Resources and Renewables, 2016). The Scotian Slope has been widely researched because of the geologic complexity of the salt tectonics around this area (Department of Natural Resources and Renewables, 2016). Various studies show how Lower and Upper Cretaceous deposits are strongly controlled by a deep-water thermogenic gas play and a probable hydrocarbon source rock is quite eminent in the slope part of this reservoir (Department of Natural Resources and Renewables, 2016). Figure 1 displays the extent of the geological setting of the Scotian Shelf, Slope and Rise off the coast of Nova Scotia.

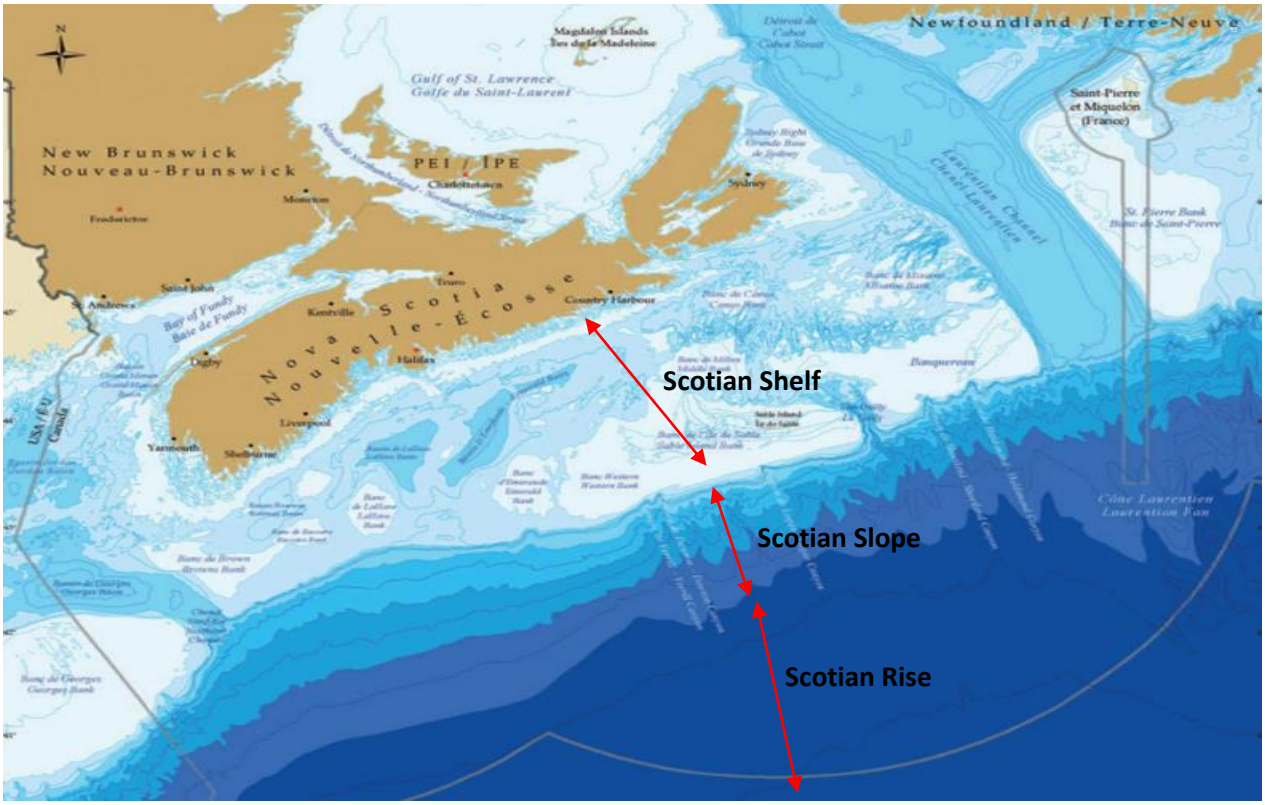

Figure 1. Geographical extent of the Scotian Shelf and the Scotian Slope (ocean depth increases from a lighter blue to a darker blue). Arrows represent rough extent of the divided zones of the Scotian Margin. (modified from Government of Canada, 2018)

1.2. Hydrocarbon seep sites

Hydrocarbon seeps are usually areas where oil and gas migrate up to the sediment water interface and these migrated hydrocarbons serve as an abundant source of nutrients and energy (Dong et al., 2020). Mostly located adjacent to continental margins, hydrocarbon seeps are regions of high metabolic microbial activity and biological productivity of chemical compound recycling (chemotrophs) that are not dependent on sunlight or photosynthesis (Harris & Baker, 2020). Salt-driven tectonics is one of the dominant processes that creates conduits through fault networks for the rapid transfer of oil, methane gas hydrates, brine pools etc. (Kennicutt et al., 1988). Reduced chemical gases from the oceanic sediment surface like H_2S and CH_4 migrate upwards from the

deeper sediments into the shallow sediments and eventually the water column (Harris & Baker, 2020). Seeps are highly productive sites of biodiversity and experience different environmental conditions and redox shifts around deep ocean sediments (Ruff, 2020). Scotian Slope studies have shown that there has been active seafloor seepage of thermogenic hydrocarbon which can be linked to the presence of an active petroleum system (Dong et al., 2020; Fowler, 2016).

1.3. Biogeochemical Cycles

Biogeochemical cycles involve the continuous and complete cycling of different elements throughout the different parts of the Earth. Biogeochemical cycles intertwine the four realms on earth, the atmosphere, biosphere, hydrosphere, and geosphere. They are driven by solar and geothermal energy and are converged at places where microorganisms to catalyze chemical reactions and exchange materials (Hedges, 1992). These cycles in turn guide the transfer, behavior and cycling of material on the Earth as well as in the oceans. Marine sediments act as one of the largest pools of accumulated organic matter throughout the world. The complex interactions between microbial communities coupled with various geochemical processes act as the driving force to break down the organic matter (Jørgensen, 2021). The six most common elements of global biogeochemical cycles are carbon, nitrogen, sulfur, hydrogen, oxygen, and phosphorus. The recycling of these elements in ocean sediments are often interconnected, and provides essential nutrients for microorganisms to help fuel their metabolism (Hedges, 1992). Ocean floor surface sediments throughout the world are host to a complex network of microbially mediated reactions that link together the carbon, sulfur, and nitrogen biogeochemical cycles. The compound cycling of these species is continuously occurring in the oceans and their concentration signatures are replicated into the porewater (PW) profiles in ocean floor surface sediments.

1.3.1. Nitrogen Cycle

Nitrogen undergoes a cyclic conversion from dinitrogen (N_2) into its various oxidized and reduced forms by a stepwise series of biological and chemical processes. In ecosystems with high organic matter accumulation and low accessibility of N_2, the capacity for chemotrophic nitrogen fixation is low (Musat et al., 2006). The reduction of atmospheric N_2 to NH_4 occurs via the process of microbially mediated N_2 fixation and is an important aspect of the global nitrogen cycle (Zehr & Capone, 1996). The cycling of NO_2^- and NO_3^- compounds are preferentially interesting for the purposes of this study. Coastal regions (like that of the Scotian Slope) are often subject to large anthropogenic forms of N_2 through detritus sedimentation among other sources (Herbert, 1999). In anoxic conditions of the deep oceanic sediments, the process of denitrification recycles NO_2^- and NO_3^- and then back into N_2 via nitrifiers (Brunnegård et al., 2004; Herbert, 1999). In marine ecosystems, about 67% of the total nitrogen production can be contributed to the low diversity of microorganisms like the anammox bacteria among others (Fernandez et al., 2011; Qian et al., 2018). The dissimilatory nitrate reduction to ammonia (DNRA) coupled with denitrification are common processes in hydrocarbon-rich sediments where microorganisms compete for NO_2^- and NO_3^- (Bonaglia, 2015). In deep oceanic sediment settings, after the exhaustion of NO_3^- is the dominant nutrient that microorganisms require to flourish and preferentially prefer to exhaust first. After the exhaustion of nitrate, the next best electron acceptor (EA) microorganisms turn to is nitrite. The exchange of nutrients in oceanic ecosystems is a useful indicator to reconstruct the presence and abundance of various anions. The increased concentration of nitrogenous compounds promotes the growth of various microorganisms and other microbially mediated fluxes.

1.3.2. Sulfur Cycle

Our knowledge and understanding of sulfur cycling and how various microorganisms guide this process is continuously developing (Wasmund et al., 2017). The sulfur cycle is largely driven by the oxidation of organic matter through sulfate-reducing microorganisms (SRM) (Jørgensen, 2021). On a global scale, recent estimates have suggested how the remineralization of up to 29% of the organic matter that is deposited on the seafloor is guided by SRM (M. W. Bowles et al., 2014). The sulfur cycling in marine sediments is globally the dominant path of anaerobic processes like dissimilatory sulfate reduction (DSR) to sulfide by various anaerobic microorganisms (Jørgensen & Kasten, 2006). DSR to S^{2-} is globally the most common pathway for organic matter mineralization in the anoxic seabed (Jørgensen et al., 2019). Sulfate (SO_4^{2-}) is the third most dominant EA in hydrocarbon enriched deep ocean sediments and microorganisms tend to turn to sulfate after the exhaustion of nitrate and nitrite. Within the oceanic sediment cycling, most of the sulfide gets re-oxidized back into sulfate via various microbially based reactions (Jørgensen et al., 2019). For a more detailed explanation of the sulfur cycling, the reader is referred to (Wasmund et al., 2017; Jørgensen et al., 2019; Jørgensen, 2021)

1.3.3. Carbon Cycle

The carbon cycle refers to the exchange of carbon as an element between the four realms on earth. The ocean is the largest place for earth's active carbon recycling (Tajika, 1999). Carbon is a unique element in its both organic and inorganic forms and its cycling includes both slow and fast components (Riebeek, 2011). The global carbon cycle describes the complex transformations and fluxes of carbon cycling variations on Earth (Carlson et al., 2001). The growth of photosynthesis allowed microbes to utilize solar energy and provide a system for the first carbon cycle to occur.

Many global ocean research programs, for example the Geochemical Ocean Sections (GEOSEC), have helped constrain the ecosystem and circulation patterns of carbon sequestration in marine systems compared to terrestrial systems (Carlson et al., 2001). Microorganisms like diatoms and phytoplankton play a crucial role in the cycling of CO_2 fixation into the organic form of carbon (Edwards et al., 2015). This organic carbon has the potential to sink into deeper depths of the ocean floor surface sediments where various microorganisms recycle it back into CO_2. The exhaustion of CO_2 is the fourth-best nutrient that acts as an EA for microorganisms. Various microorganisms then cause the dissolution of CO_2 to form carbonate. Various studies suggest that seep CO_3^{2-} formation is also controlled by the hydrocarbon flux changes around the sulfate methane transition zone (SMTZ) (Roberts, 2001). For this study, we are most interested in CO_3^{2-} cycling through the ocean floor sediments and how it behaves concerning the other anions around it.

1.4. Redox Gradients

Redox gradients form when reduction-oxidation settings are produced in closed systems. Redox gradients are fairly common in oceanic shallow sediments (Barge et al., 2019). There is a continuous diffusion between the upper water column and ocean floor mud pore spaces. Biogeochemical processes occurring in the upper sediment column show a distinct vertical pattern concerning the ion geochemistry in these zones (e.g. Figure 2 from Jilbert, 2016). The changes in oceanic sediment redox chemistry can frequently be observed throughout the Earth's history (Van de Velde et al., 2020). Reconstruction of this vertical zonation can prove difficult due to the shortage of Cretaceous rock records displaying definite deposition in the deep-sea environments (van de Velde et al., 2020). These redox gradients are led by various microbial activities and processes like AOM and DSR which cause the shifts in their ion redox chemistry and leads to the

formation of biogeochemically controlled redox gradients. These redox gradients play an important role in guiding the anion geochemistry of marine sediments.

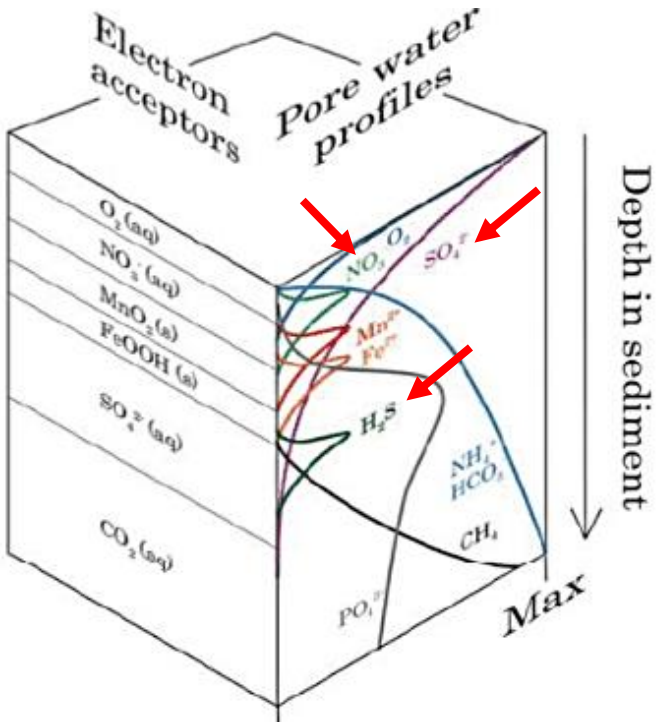

Figure 2. Diagram showing an idealized electron tower redox reaction succession in marine conditions and how the ion chemistry changes with increasing depth. Red arrows point toward elements of interest for this study. (modified from Jilbert, 2016)

1.5. Porewater

Porewater (PW) trapped in between marine sediments can be a valuable tool to reconstruct the nature and kinetics of diagenetic reactions that occur as sediments get buried at depth (Di Bonito et al., 2018). Any change in the chemistry of sediments is directly emanated into the quantitative PW concentrations. For studies around the geochemical cycling of trace elements in deep oceanic sediments, the analysis of PW is more helpful than soil sampling studies (Hammond, 2001). Porewater chemistry is largely controlled by the prevailing pathways of organic matter remineralization in the deep oceanic surface sediments (Jilbert, 2016). The PW trapped in between

the marine sediment particles is capable of emitting the redox zonation of different anions and cations (Figure 2). For every observed concentration gradient, a corresponding vertical flux of PW can be reconstructed (Schulz, 2006). While the exact concentration of the redox diversity of the deep ocean can be difficult to reconstruct, measuring the concentration through PW can bring us quite close to the expected pattern (van de Velde et al., 2020).

1.6. Ion Chromatography (IC)

Ion chromatography has widely been an essential tool for analytical chemistry. The highly sensitive technique typically is based on a combination of gradients and a suppressed conductivity detection system coupled with high-performance stationary phases that makes it ideal for chemical water analysis (Nesterenko & Paull, 2017). Ion chromatography is extensively used for monitoring the contaminants in drinking water (Rohrer, 2019). For water samples that contain the appreciable level of common cations and anions, like Ca and Mg or NO_2^-, NO_3^-, and SO_4^{2-}; IC has proved itself to be the preferred method to measure and reconstruct their concentration analysis (Pohl, 2005). This is a form of liquid chromatography that measures the concentration of organic/inorganic ions based on their interaction with an ion-exchange column coupled with a conductivity detector (Haddad, 2000). Before injection of a sample, pre-treatment with in-line cartridges is required to provide a lower baseline, better separation and to eliminate matrix interferences. When a sample of the mixture is prepared, it goes through different components in an IC system before reaching the chromatograph (Figure 3).

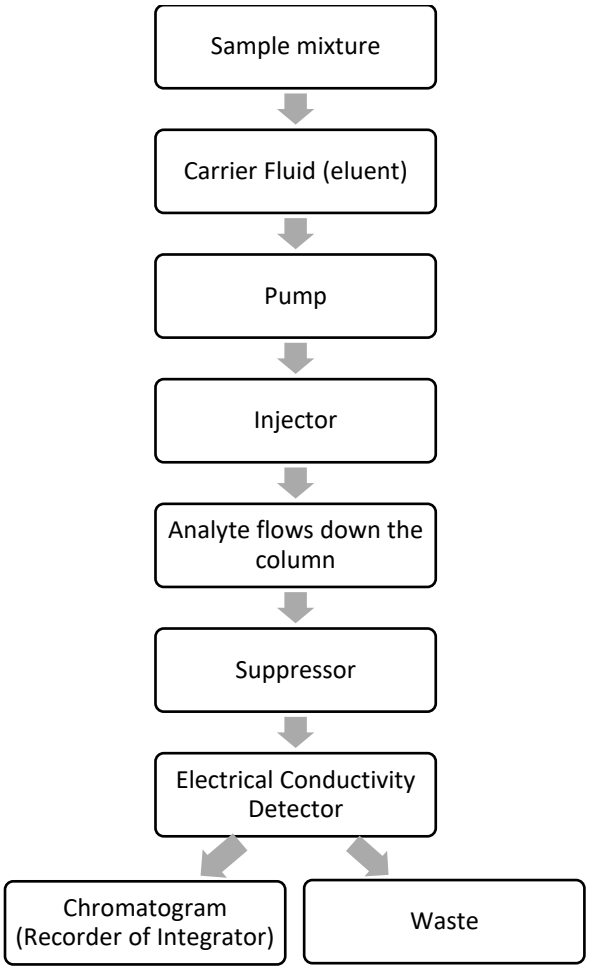

Figure 3. Flow diagram showing the instrumental components of an IC (modified from Nesterenko & Paull, 2017) .

1.7. Standard Addition Method

The standard addition method is based on adding consecutively increasing standard dilutions to the unknown analyte to compensate for sample constituents that might enhance or suppress a signal and measuring the solution's analytical signals in response to each respective addition (Saxberg & Kowalski, 1979). It is often also known as ‘spiking’ the sample to a known matrix and baseline (Andersen, 2017). The standard addition is a commonly used technique for quantitative chemical

analysis and to overcome matrix interferences for a sample (Saxberg & Kowalski, 1979). The calculation of the standard addition method involves the assumption of homogeneity of variance and that only the data is rarely scattered by the presence of foreign elements while the analytical signal value will solely be based upon regression standard equations (Rodríguez et al., 1995). At least three to four standard addition dilution mixtures are prepared to calibrate the analytical method and to assess the recovery of the analytes with the use of regression equations (example Appendix A, Figure A2) (Pastore et al., 2005). An advantage to using standard addition is that it does not require a blank matrix for measuring the quantity of a target compound while a common disadvantage of the experiment is that it is labor-intensive process (Hasegawa et al., 2021).

1.8. Calibration Curve Method

Calibration curve is another external chemical analytical technique that can commonly be used for ion chromatographic analysis to calculate the recovery of the net signal obtained through the continuous addition of standard injections (Gámiz-Gracia et al., 2003). It is an external calibration analytical method used to calculate the analyte content, recovery and sensitivity of analytical signals (Saxberg & Kowalski, 1979). It is based on producing a standard set of regression equations through continuous injections of different standard dilutions to the chromatograph and integrating the analytical signals to those standard sets of equations. Although this method is less time-consuming, however a standard set of assumptions are applied in this method which increases the chances of error, for example, if the linear range of the detector is not taken into consideration, it could lead to inaccurate results (Büttner et al., 1977).

1.9. Research Objective and Hypothesis Statement

Ocean floor surface sediments of the Scotian Slope are host to a complex network of microbially mediated reactions that knit together the carbon, sulfur, and nitrogen biogeochemical cycles. Within PW, these elements are complexed as a series of ions that are microbially generated and/or shuttled across sediment depths by diffusion and microbial respiratory processes. Major PW ionic species may display different stratigraphic trends in hydrocarbon impacted marine sediments. Limited diffusion between the upper water column and ocean floor muds pore space, coupled with competitive microbial ecological niche partitioning, leads to the formation of biogeochemically controlled redox gradients (Figure 2). These redox gradients play an important role in guiding the anion geochemistry of the marine sediments of the Scotian Slope. We hypothesize that the PW anions as F^{-}, NO_2^{-}, NO_3^{-}, CO_3^{2-}, and SO_4^{2-} extracted from frozen marine sediment cores located in prospective hydrocarbon seep sites of the Scotian Slope can be used to reconstruct biogeochemical stratification depth profiles that can provide comparative evidence for anion behaviour in active cold seep sites.

2. Experimental

2.1. Instrument and Sample Preparation Equipment

Anion chromatographic analysis was performed using a Thermo Scientific Dionex Aquion Ion Chromatography Conductivity Detector System with an anion-exchange column and a DS6 Heated Conductivity Cell fitted with an AERS_4mm suppressor pump and a Dionex AXP Auxiliary pump and pump ECD. The ion chromatograph is further configured with an in-line Thermo Scientific 9×24mm Dionex InGuard Ag sample prep cartridge and Thermo Scientific Dionex InGuard Na prep cartridge to facilitate trace analysis of seawater. The IC is controlled via Thermo Scientific Chromeleon 7 chromatography system version 7.3 software. An Elma 5300 ElmaSonic Sonicator

and Beckman Coulter Avanti J-15 Centrifuge were used for sample sonication and centrifugation during sample preparation.

2.2. Reagents and Chemicals

The solvent used in this study was Thermo Fisher Scientific Deionized HPLC ACS reagent grade water, ASTM Type 1 (100%, CAS# 7732-18-5) stored at room temperature. The mobile phase was 25mM NaOH 50% w/w solution from Fisher Chemicals SS254-1, stored in a cool, dark place. The chemicals used for the standard addition and the calibration curve method were all analytically pure and prepared with the use of Thermo Scientific Dionex Seven Anion Standard II (from Sunnyvale, California) in deionized water. The anion standard (S+D) was an amalgamation of H_2O (99.9%, CAS# 7732-18-5) and the following anions – F^- (20mg/L, CAS# 7681-49-4); Cl^- (100mg/L, CAS# 100mg/L); NO_2^- (100mg/L, CAS# 7632-00-0); Br^- (100mg/L, CAS# 7647-15-6); NO_3^- (100mg/L, CAS# 7631-99-4); PO_4^{3-} (200mg/L, CAS# 7778-77-0); SO_4^{2-} (100mg/L, CAS# 7757-82-6) , stored in -4 °C refrigerator. Carbonate and Sulfite are prepared as separate stock solutions. Carbonate is prepared using Anhydrous Sodium Carbonate ACS powder from Fisher Chemicals (CAS # 497-19-8) and SO_3^{2-} is prepared using Anhydrous Sodium Sulfite crystalline powder from Fisher Chemicals (CAS# 7757-83-7).

3. Methodology

3.1. Preparation of Mobile Phase

For the mobile phase, 25 mM of NaOH chemical was diluted with HPLC grade water to ensure better separation and resolution of anion signals. Hence, for 1L of HPLC grade water, 1.308 mL

of NaOH was required. After mixing NaOH with the water, the solution was sonicated for 5 min. before use.

3.2. Preparation of Standard

To prepare 2000 mg/L (ppm) stock solution of CO_3^{2-}, 88.310mg of anhydrous sodium carbonate powder is mixed with 25 mL HPLC grade water and stored in -4 °C refrigerator. To prepare 2000 mg/L stock solution of SO_3^{2-}, 80.322mg of sodium sulfite is mixed with 25mL HPLC grade water and stored in -4 °C refrigerator. To prepare 2 mL of standard for standard addition dilution, for the initial set of samples, two different standard concentrations were prepared. For the initial set of samples, 20 ppm S+D, 20 ppm SO_3^{2-} , and 20 ppm CO_3^{2-} . For the latter set of samples, 50 ppm S+D, 0 ppm SO_3^{2-} , and 500 ppm CO_3^{2-} . Please refer to Appendix A for full information. For each anion concentration, at least 3-4 different standard addition dilution calibration were prepared. For the initial set of samples, it was assumed that the sediments also host some concentration of SO_3^{2-} , hence the prepared stock solution of SO_3^{2-} was added to the standard but was discarded later when almost no concentration of the anion was found in the sediment samples. Please refer to Appendix A for full information on which samples had SO_3^{2-} added to the standard dilution.

3.3. Ion Chromatographic Analysis

Prior to IC analysis, samples were pre-treated by cartridges. An in-line Ag sample prep cartridge was used in the IC system to removes halides such as Cl^-, Br^-, and I^- from sample matrices. The Thermo Scientific Dionex InGuard Na cartridges were also used to remove alkaline metals from sample matrices and to facilitate trace analysis. The Dionex AXP Auxiliary Pump that is used to

pump water through the inline cartridge runs at a flow rate of 1.00 mL/min with pressure ranging from 0 -3000psi while the Pump ECD runs at a flow rate of 1.50 mL/min.

3.4. Sediment Porewater

The ocean floor surface sediments were obtained from the deep marine hydrocarbon seep sites along the Scotian Slope and were stored in -80 ° C immediately upon collection. A total of 50 frozen sediment samples spread out over nine spatially different cores were analyzed for the purpose of anion chromatography. Among these, there were 17 shallow push cores, 8 deeper gravity cores and 25 deeper piston cores. These sediments were extracted on cruises in July 2015, 2016, 2018 and 2021. The anions of interest for this study are F^{-}, NO_2^{-}, NO_3^{-}, CO_3^{2-} , SO_3^{2-}, and SO_4^{2-}. For each frozen sediment sample, 30 – 35 mg of sediment was extracted and transferred to 50 mL centrifuge tubes and shut tight to avoid contamination via air. This sediment was left at room temperature for 40–50 min to thaw followed by high-speed centrifugation at 2000 rpm for 10–15 min until the sediment and the PW physically separated. The PW was then extracted and filtered using a disposable filter and syringe to remove the micro sized sediment particles and to obtain a cleaner aliquot of PW.

3.5. Standard Addition Methodology

The PW sample was then subject to the method of standard addition dilution where a specific amount of standard is added to the extracted PW in concentrations of 0, 2, 5, 10 and 20 ppm. For the 2015, 2016 and 2018 samples, the mixture of standard addition used is specified in Table 1. For the 2021 samples, the mixture of standard addition dilution used is specified in Table 2. Not

all the samples were subject to the same amount of standard addition injections and that it was a continuously evolving process. For example, the addition of 20 ppm standard dilution was adopted to create a better separation between the different dilution signals. For full information of the specifications of the methodology please refer to table A2, Appendix A. Before the prepared solutions were injected into the instrument, 3-4 Blanks were run to flush out the column, followed by a run of 5 ppm (HPLC water dilution) of the prepared standard. The run time in the program for each sample in a section is approximately 20 min where the program produces peak signal area with respect to time and micro siemens (conductance).

Table 1. Amount of PW, Standard Mix and HPLC grade water mixed to obtain each injection for the initials et of samples.

Dilution + Standard Addition	Filtered PW (µL)	20ppm Standard Mix (µL)	HPLC grade water (µL)	Total Volume (µL)
10x + 0ppm	60	0	540	600
10x + 2ppm	60	60	480	600
10x+ 5ppm	60	150	390	600
10x +10ppm	60	300	240	600

Table 2. Amount of PW, Standard Mix and HPLC grade water mixed to obtain each injection for the latter set of samples.

Dilution + Standard Addition	Filtered PW (µL)	50ppm Standard Mix (µL)	HPLC grade water (µL)	Total Volume (µL)
10x + 0ppm	60	0	540	600
10x + 5ppm	60	60	480	600
10x+ 10ppm	60	120	420	600

10x +20ppm	60	240	240	600

3.6. Calibration Curve methodology

Standards having the concentration of 0.5, 1, 2, 5, 10, 20 and 50 ppm were injected into the IC to produce a standard set of regression equations (specified in Table 3). The area produced by the peaks concerning time and micro siemens is further integrated and a single regression equation is produced for each anion. For each sample run under different standard addition dilutions of 10x + 0 ppm, 10x + 2 ppm, 10 x +5 ppm, 10x + 10 ppm, 10x + 20 ppm, the area obtained from the 10x + 0 ppm run was used and inserted into the following regression equations.

Table 3. Regression equations produced for the calibration curve method.

Anions	Calibration Curve Equations
Fluoride	Signal (F^-) = 0.2531 (F^-) - 0.0176
Nitrite	Signal (NO_2^-) = 0.1087 (NO_2^-) - 0.0271
Carbonate	Signal (CO_3^{2-}) = 0.0025 (CO_3^{2-}) + 0.0079
Sulfate	Signal (SO_4^{2-}) = 0.2178 (SO_4^{2-}) - 0.0372
Nitrate	Signal (NO_3^-) = 0.0828 (NO_3^-) - 0.0268

3.7. Data Analysis

For both standard addition and calibration curve, the data analysis is similar. While for standard addition, after a blank was subtracted from each peak signal, the area obtained for each anion in each sample was further integrated using the regression equations produced for the line of best fit

by substituting the y coordinate as zero and solving for x coordinate (Figure A2, Appendix A). For the calibration curve, the standard regression equations produced (Table 3) were used in a similar way. For both methods, the area produced was further multiplied by 10 to revert to the ×10 dilution that the PW was subject to at the time of sample preparation. This area was then used to plot the depth v/c concentration plots.

4. Results and Discussion

Nova Scotia has been actively researching and surveying potential hydrocarbon seep sites along the deep-water Scotian slope to research its hydrocarbon potential. Figure 4 provides the location of piston, gravity and push cores spatially separated across the extent of the Scotian Slope associated with a Genome Application Partnership Program (GAPP) that has been active since 2015. Sites circled in red have been used for this study. A total of 50 frozen sediment samples spread across nine cores were used to gather data for this study. Table 4 contains the sample collection year, core number, archived sample name, depth, geographic core location and their expected hydrocarbon positive/negative behaviour. Table 5 and Table 6 provides the concentration of anions measured across these cores with the method of standard addition and calibration curve respectively.

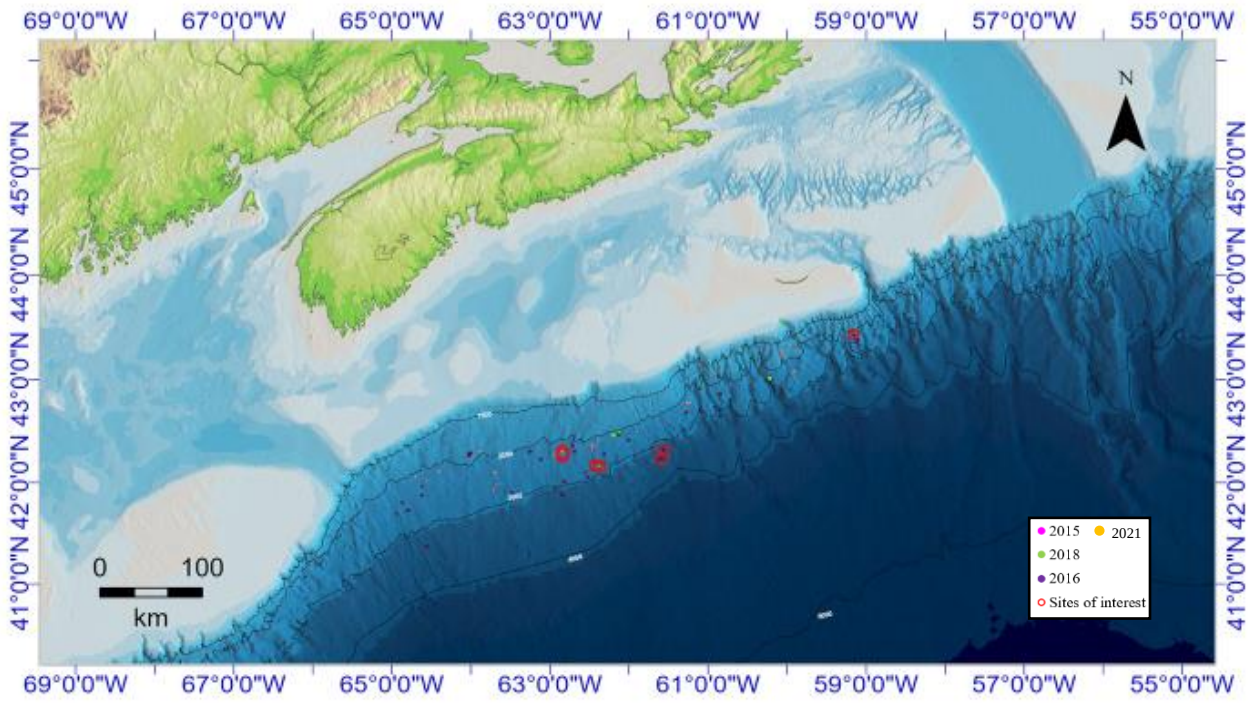

Figure 4. Geological setting of the Scotian Slope and the location of all the collected cores and when they were drilled. Sites of interest for this study are circled in red.

Table 4. Geographic location of samples and detected presence of hydrocarbons.

Year	Core	Archived Sample Name	Depth		Geographic Location		Hydrocarbon Behaviour
			Range	Exact	Latitude	Longitude	
2015	**9**	NSPC 2015018-0009 S01 B 144-149cm	144-149 cm	144	42.308610	-62.836325	Positive
		NSPC 2015018-0009 S03 B 297-302cm	297-302 cm	297	42.308610	-62.836325	Positive
		NSPC 2015018-0009 S04 B 363-369cm	363-369 cm	363	42.308610	-62.836325	Positive
2016	**49**	2016011-049 S01 B 77-82cm	77-82 cm	77	42.159815	-62.359746	Positive
		2016011-049 S02 B 144-149cm	144-149 cm	144	42.159815	-62.359746	Positive
		2016011-049 S03 B 226-231cm	226- 232 cm	226	42.159815	-62.359746	Positive

		2016011-049 S04 B 362-367m	362- 367 cm	362	42.159815	-62.359746	Positive
		2016011-049 S05 B 403-409cm	403-409 cm	403	42.159815	-62.359746	Positive
		2016011-049 S07 B 460-465cm	460-465 cm	460	42.159815	-62.359746	Positive
		2016011-049 S08 B 620-625cm	620- 625cm	620	42.159815	-62.359746	Positive
	21	2016011-021 S01 B 12-17cm	12-17 cm	12	42.308531	-62.838306	Positive
		2016011-021 S02 B 148-155cm	148-155 cm	148	42.308531	-62.838306	Positive
		2016011-021 S03 B 210-215cm	210-215 cm	210	42.308531	-62.838306	Positive
		2016011-021 S04 B 230-236cm	230-236 cm	230	42.308531	-62.838306	Positive
		2016011-021 S05 B 250-255cm	250-255 cm	250	42.308531	-62.838306	Positive
		2016011-021 S06 B 285-290cm	285-290 cm	285	42.308531	-62.838306	Positive
	32	2016011-032 S01 B 260-265cm	260-265 cm	260	42.234850	-61.599353	Positive
		2016011-032 S02 B 385-390cm	385-390 cm	385	42.234850	-61.599353	Positive
		2016011-032 S03 B 540-545cm	540-545 cm	540	42.234850	-61.599353	Positive
	33	2016011-033 S01 B 170-175cm	170-175 cm	170	42.317898	-61.566376	Negative
		2016011-033 S02 B 320-325cm	320-325 cm	320	42.317898	-61.566376	Negative
		2016011-033 S03 B 610-615cm	610-615 cm	610	42.317898	-61.566376	Negative
	44	2016011-044 S01 B 432-437m	432-437 cm	432	43.435396	-59.152075	Negative
		2016011-044 S02 B 601-606cm	601-606 cm	601	43.435396	-59.152075	Negative
		2016011-044 S03 B 755-760cm	755-760 cm	755	43.435396	-59.152075	Negative
2018	**13**	2018041-0013 gc 5-15cm	5-15cm	5	42.162286	-62.355680	Negative

		2018041-0013 gc 58-62 cm	58-62cm	58	42.162286	-62.355680	Negative
		2018041-0013 gc 190-195cm	190-195cm	190	42.162286	-62.355680	Negative
		2018041-0013 gc 255-260cm	255-260cm	255	42.162286	-62.355680	Negative
		2018041-0013 gc 315-320 cm	315-320cm	315	42.162286	-62.355680	Negative
		2018041-0013 gc 420-425cm	420-425cm	420	42.162286	-62.355680	Negative
		2018041-0013 gc 533-538cm	533-538cm	533	42.162286	-62.355680	Negative
		2018041-0013 gc 570-575cm	570-575cm	570	42.162286	-62.355680	Negative
2021	**1-46D**	46D 0-2cm	0-2cm	0	43.010208	-60.212067	Positive
		46D 4-6cm	4-6cm	4	43.010208	-60.212067	Positive
		46D 8-10cm	8-10cm	8	43.010208	-60.212067	Positive
		46D 10-12cm	10-12cm	10	43.010208	-60.212067	Positive
		46D 14-16cm	14-16cm	14	43.010208	-60.212067	Positive
		46D 16-18cm	16-18cm	16	43.010208	-60.212067	Positive
		46D 20-22cm	20-22cm	20	43.010208	-60.212067	Positive
		46D 24-26cm	24-26cm	24	43.010208	-60.212067	Positive
		46D 28-30cm	28-30cm	28	43.010208	-60.212067	Positive
	1-9A	9A 0-2 cm	0-2cm	0	43.010795	-60.213159	Negative
		9A 4-6cm	4-6cm	4	43.010795	-60.213159	Negative
		9A 8-10cm	8-10cm	8	43.010795	-60.213159	Negative
		9A 12-14cm	12-14cm	12	43.010795	-60.213159	Negative

	9A 16-18cm	16-18cm	16	43.010795	-60.213159	Negative
	9A 20-22cm	20-22cm	20	43.010795	-60.213159	Negative
	9A 22-26cm	22-26cm	22	43.010795	-60.213159	Negative
	9A 30-34cm	30-34cm	30	43.010795	-60.213159	Negative

Table 5. Standard addition determined anion concentrations.

Standard Addition Data									
Year	**Core**	**Depth**		**Concentration of Anions (ppm)**					
		Range	**Exact**	**Fluoride**	**Nitrite**	**Carbonate**	**Sulfite**	**Sulfate**	**Nitrate**
2015	Core 9	144-149 cm	144	1.9	0.0	145.7	0	4020.8	0.3
		297-302 cm	297	1.4	0.0	182.4	0	1772.5	1.3
		363-369 cm	363	1.4	0.2	439.3	0	40.9	1.8
2016	Core 49	77-82 cm	77	0.8	0.0	202.2	0	845.2	1.9
		144-149 cm	144	1.0	3.9	457.3	0	119.5	0.4
		226- 232 cm	226	1.8	2.9	623.2	0	106.5	0.3
		362- 367 cm	362	1.0	0.5	528.8	0	146.1	0.5
		403-409 cm	403	1.1	6.7	496.3	0	49.1	3.7
		460-465 cm	460	0.9	0.4	887.3	0	24.1	1.0
		620- 625cm	620	0.5	4.6	443.0	0	8.2	3.7

	Core 21	12-17 cm	12	1.3	0.0	201.7	0	1607.2	1.3
		148-155 cm	148	1.4	0.0	570.4	0	181.1	0.9
		210-215 cm	210	0.9	0.7	770.5	0	200.6	0.7
		230-236 cm	230	0.4	0.9	776.8	0	224.8	0.5
		250-255 cm	250	1.1	0.0	1649.0	0	237.3	0.3
		285-290 cm	285	1.2	0.0	2075.6	0	50.6	1.1
	Core 32	260-265 cm	260	1.4	0.0	147.5	0	2119.4	2.9
		385-390 cm	385	1.4	0.0	161.3	0	933.9	0.7
		540-545 cm	540	1.3	0.0	192.6	0	1782.4	2.0
	Core 33	170-175 cm	170	2.0	0.0	152.5	0	1401.2	1.5
		320-325 cm	320	1.7	0.0	231.6	0	1005.7	2.1
		610-615 cm	610	1.7	0.1	435.7	0	1579.9	0.8
	Core 44	432-437 cm	432	0.9	0.0	365.0	0	955.7	6.0
		601-606 cm	601	1.1	0.0	490.4	0	838.7	9.2
		755-760 cm	755	0.9	0.0	538.5	0	380.8	0.5
2018	Core 13	5-15cm	5	0.6	5.7	69.5	0	1131.3	19.0
		58-62cm	58	2.3	8.0	411.1	0	1077.7	1.4
		190-195cm	190	0.7	23.0	357.2	0	638.3	9.3
		255-260cm	255	0.5	26.0	314.5	0	694.2	4.7
		315-320cm	315	0.8	23.2	325.9	0	1589.2	5.5

		420-425cm	420	0.8	24.9	412.6	0	1090.1	5.0
		533-538cm	533	0.1	16.2	613.2	0	1382.7	13.0
		570-575cm	570	0.6	16.4	515.2	0	1965.6	10.3
2021	Core 1-46D	0-2cm	0	0.1	0.5	175.9	0	961.0	6.8
		4-6cm	4	0.8	10.8	480.0	0	1954.7	39.5
		8-10cm	8	1.3	17.4	401.0	0	1700.9	24.6
		10-12cm	10	0.3	25.4	418.5	0	1105.7	49.2
		14-16cm	14	0.1	1.4	179.2	0	1827.6	17.5
		16-18cm	16	1.8	24.4	496.2	0	1583.3	46.7
		20-22cm	20	1.1	26.4	837.3	0	2189.4	31.5
		24-26cm	24	0.3	4.9	289.3	0	1351.6	31.6
		28-30cm	28	0.4	15.4	411.0	0	3065.2	31.5
	Core 1-9A	0-2cm	0	0.3	26.3	787.5	0	1819.4	35.3
		4-6cm	4	0.4	29.3	748.4	0	2230.7	41.4
		8-10cm	8	1.2	34.5	678.1	0	1700.1	31.0
		12-14cm	12	1.5	23.9	1022.9	0	1474.0	31.6
		16-18cm	16	1.0	29.7	1436.2	0	2177.0	26.2
		20-22cm	20	1.1	27.7	675.6	0	1658.5	36.9
		22-26cm	22	1.4	29.3	660.7	0	1426.0	27.6
		30-34cm	30	0.8	24.0	564.8	0	1300.8	27.2

Table 6. Calibration curve determined anion concentrations.

Calibration Curve Data									
Year	Core	Depth		Concentration of Anions (ppm)					
		Range	Exact	Fluoride	Nitrite	Sulfite	Carbonate	Sulfate	Nitrate
2015	Core 9	144-149 cm	144	2.2	2.5	0	143.2	1375.2	3.2
		297-302 cm	297	1.7	2.5	0	180.0	697.5	4.4
		363-369 cm	363	1.8	2.7	0	478.0	24.2	4.8
2016	Core 49	77-82 cm	77	1.8	2.5	0	194.4	1350.7	3.2
		144-149 cm	144	1.9	5.4	0	645.2	85.9	3.2
		226- 232 cm	226	1.4	4.0	0	666.4	66.0	3.2
		362- 367 cm	362	1.9	3.5	0	687.6	89.8	6.0
		403-409 cm	403	2.0	9.8	0	566.4	29.1	3.2
		460-465 cm	460	1.8	4.0	0	500.4	17.6	3.2
		620- 625cm	620	1.6	8.6	0	376.0	8.1	3.2
	Core 21	12-17 cm	12	1.7	2.5	0	215.2	1149.9	3.2
		148-155 cm	148	2.6	2.5	0	551.2	127.6	3.2
		210-215 cm	210	1.8	3.2	0	578.8	125.4	4.8

		230-236 cm	230	1.2	4.6	0	570.0	137.8	5.4
		250-255 cm	250	1.8	2.5	0	625.6	113.2	3.2
		285-290 cm	285	2.3	2.5	0	713.2	33.6	3.2
	Core 32	260-265 cm	260	1.8	2.5	0	157.2	1469.2	3.2
		385-390 cm	385	1.7	2.5	0	174.8	1369.6	3.2
		540-545 cm	540	1.6	2.5	0	207.2	1320.9	3.2
	Core 33	170-175 cm	170	1.8	2.5	0	139.2	1444.7	3.2
		320-325 cm	320	1.9	2.5	0	200.0	1349.1	3.8
		610-615 cm	610	1.9	2.5	0	334.4	1044.1	4.0
	Core 44	432-437 cm	432	1.8	2.5	0	366.8	861.3	3.2
		601-606 cm	601	1.7	2.5	0	481.2	561.2	3.2
		755-760 cm	755	1.7	2.5	0	520.0	335.6	5.5
2018	Core 13	5-15cm	5	1.4	9.7	0	51.6	1245.2	19.1
		58-62cm	58	2.8	10.6	0	236.8	1272.4	4.2
		190-195cm	190	1.4	21.1	0	186.8	1131.5	13.8
		255-260cm	255	1.3	26.0	0	304.0	1248.2	6.6
		315-320cm	315	1.4	23.9	0	294.8	1141.1	7.4
		420-425cm	420	1.5	26.5	0	393.2	999.5	6.6

		533-538cm	533	1.1	18.1	0	384.0	796.4	15.0
		570-575cm	570	1.3	18.3	0	386.0	731.9	14.2
2021	Core 1-46D	0-2cm	0	1.7	4.2	0	183.2	1310.8	18.0
		4-6cm	4	2.0	12.2	0	133.6	1433.9	49.4
		8-10cm	8	2.0	23.5	0	110.4	1560.9	29.3
		10-12cm	10	1.8	30.0	0	503.6	1452.7	57.9
		14-16cm	14	1.7	6.8	0	228.0	1507.5	28.6
		16-18cm	16	1.9	28.7	0	405.6	1581.4	57.5
		20-22cm	20	2.2	35.4	0	720.0	1614.8	42.0
		24-26cm	24	1.5	10.9	0	284.4	1444.1	45.0
		28-30cm	28	1.7	18.1	0	576.0	1378.4	38.5
	Core 1-9A	0-2cm	0	2.0	34.4	0	693.6	1499.5	44.3
		4-6cm	4	1.8	34.3	0	692.0	1530.1	47.9
		8-10cm	8	2.4	42.5	0	654.0	1506.7	46.8
		12-14cm	12	2.4	27.7	0	946.8	1535.4	42.7
		16-18cm	16	2.4	36.6	0	1103.2	1537.4	33.0
		20-22cm	20	2.3	36.4	0	762.8	1506.7	48.9
		22-26cm	22	2.7	39.4	0	648.4	1491.6	38.8

30-34cm	30	1.9	31.5	0	506.4	1502.9	34.5

4.1. Comparative study of standard addition and calibration curve methods

Both standard addition (internal calibration method) and the calibration curve method (external calibration method) have advantages and disadvantages. Therefore, a comparative study was carried out and the data obtained from both methods was plotted on x-y scatter plot of depth versus concentration (Figure 5 (a-e)). A trendline was plotted for each anion and each method and the percent difference as proxy for variance was calculated out for each anion to measure the shift of values between the two methods. Fluoride concentrations (Figure 5a) were low, ranging between 0–3 ppm and are uncorrelated with sediment depth ($R^2 = 0.00$) with increasing sediment depth for the method of standard addition. In slight contrast, a poor negative correlation ($R^2 = 0.17$) is observed with the calibration curve method. For F^-, the shift in the values for the calibration curve method with respect to the standard addition method was ~45%. Nitrite concentrations (Figure 5b) are higher and range from 0–45 ppm and almost all of the Scotian Slope samples display similar down core trends; however, there is a slight shift towards an increased concentration for the calibration curve method ~25%. Nitrate concentrations (Figure 5c) range between 0–60 ppm and record slightly elevated values for the calibration curve method. The NO_3^- concentration plotted with depth has the highest $R^2 = 0.42$ compared to all other surveyed anions. Carbonate concentrations (Figure 5d) are nearly comparable for both methods except for some higher concentration outliers (highlighted in a red circle) that are evident in the standard addition method. Both outliers belong to core 21, a hydrocarbon positive site. Sulfate concentration trend (Figure

5e) is almost similar for both methods but there is a shift towards a decreased concentration for the calibration curve method. Previous studies suggest that the Scotian Slope surface sediments are rich in sulfur compounds, hence the method of calibration curve indicating a lower sulfate concentration seems puzzling (Cranston, 1994; Grant et al., 1998). In addition to the anions of interest, PW solutions are a matrix that generally include salts, anions, cations, organic acids, and particulate and dissolved organic carbon (POC and DOC, respectively). These species must be removed from the matrix to improve the quality of signal. But sometimes, some species end up passing through the detector and their signal can interfere with our baseline signal. This phenomenon is commonly known as a 'matrix effect'. Two possibilities explain the matrix effect in anion concentration offsets and the presence of outliers across the two methods. The first is sensitivity to anion concentration where greater offset may occur due to very high or low abundant anions. Evidence for this is the large opposing offset of the F^- anion that could be attributed to its extremely low concentration. Smaller analytes also produce larger variance. To test this possibility, the average, standard deviation, and variance percentage of each anion was calculated (full information in Table B1, Appendix B). It was noted that there is an approximate 20% offset in all the anions which measured above a certain concentration while for F^-, there was an approximate 45% offset in the negative direction. Although from a macroscopic perspective it would appear that the concentration of the anions has an immense control on performance of the standard addition and calibration curve measurement, it was also noticed that the variations in concentration also seem to be constantly changing as a function of sediment depth and that the shallow samples show a greater disparity than the deeper samples. For example, for F^-, the calibration offsets range from -1.79 to 0.46 (Table B1, Appendix B) with more negative offsets belonging to the more recently acquired shallow push core samples. Therefore, evidently the second possibility being

that the offset could be sample specific and the sample itself has unique characteristics that are introducing the higher matrix effects. For example, the trends in figure 5 seem to indicate that the offsets can go either direction positive or direction negative. Additionally, it appears the trend of standard addition versus calibration curve has more stratigraphic controls on the performance. For example, the low concentration of SO_4^{2-} produces a higher offset in shallow sediments but almost no offsets in deeper sediments. Hence in conclusion, the matrix effect appears to be either sample specific or the combination of concentration dependent and sample specific. Lastly, the offsets could then be attributed to interesting phenomena in each individual cores. Calibration curve method is generally reliable when the signal is directly proportional to the concentration and a linear trend can be expected from the unknown samples (Brinkmann et al., 2002). For unknown samples that might have higher/lower concentration ranges than expected, calibration curve extrapolation quickly becomes non-linear and a regular regression equation is not useful anymore (Brinkmann et al., 2002). For example, being a low concentration anion, it would seem like F^- has a lower susceptibility to matrix effects than the highly saturated SO_4^{2-} anion. In this regard, the low concentration anions would be harder to measure with the calibration curve technique because the signal is more prone to undergo signal suppression due to the matrix effect. For measurements where the response of the instrument cannot be controlled and the sample has the probability to have a rather complex matrix the standard addition method is more useful (Zenkevich & Klimova, 2006). Based on the reasons indicated, the method of standard addition appears more appropriate for our data involving complex matrices and concentrations ranging close to zero and as high as 5000 ppm. Therefore, the rest of the data interpretation is based on the data measured from the method of standard addition.

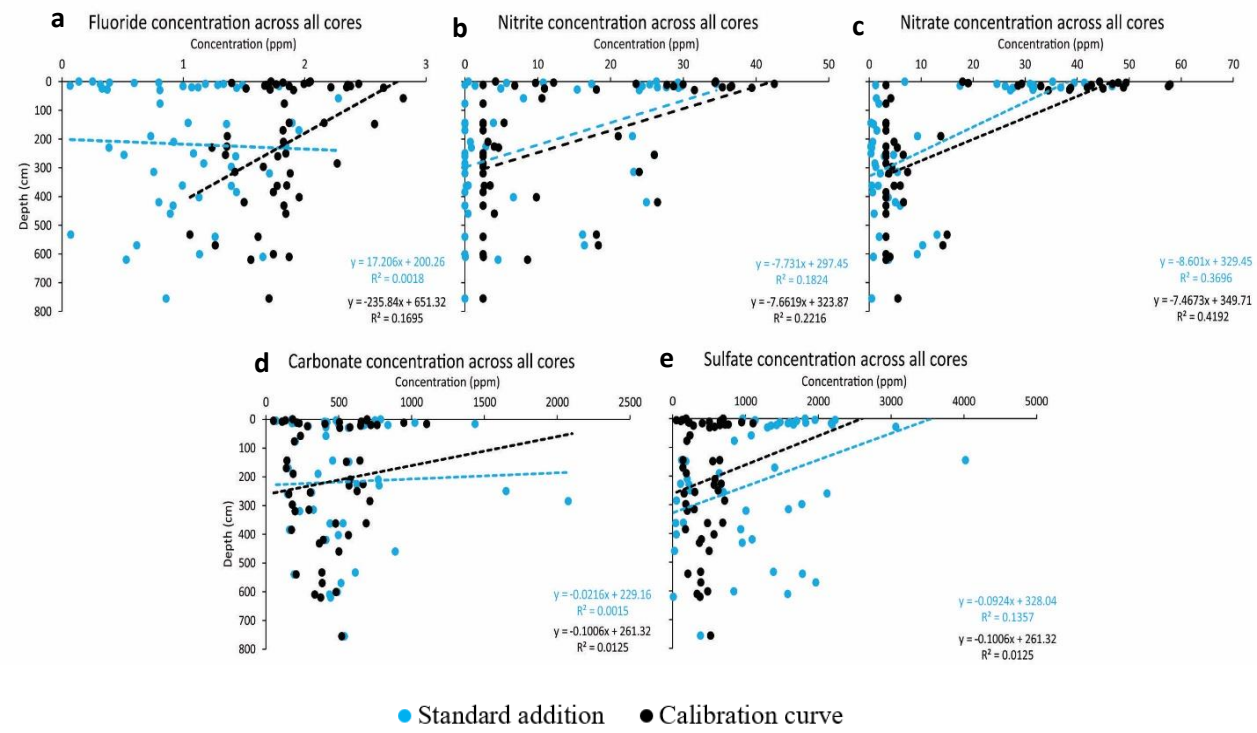

Figure 5 (a-e). Comparison of standard addition (blue) versus calibration curve (black) data for different anion concentrations.

4.2. Porewater concentration as a function of ocean floor surface sediment depth

4.2.1. Scotian Slope core survey

Ocean floor sediment PW's have distinct anion concentrations. Figure 6 (a-e) displays the individual anion concentrations plotted against their depth in centimeters below seafloor (cmbsf). The lowest concentration anion is F^-, followed by NO_2^- , NO_3^-, CO_3^{2-} and SO_4^{2-}. Fluoride ranges between 1–3 ppm and is uncorrelated with sediment depth (Figure 6a). No indication of a specific pattern for F^- indicates further studies are required to produce a better fit for a halide dependent standard addition method. Nitrite concentrations range between 0–35 ppm and on average decrease with sediment depth (Figure 6b). Outliers in deeper sediments are highlighted with a red circle and

entirely belong to the hydrocarbon positive core 49 and hydrocarbon negative core 13. The highest NO_2^- concentration measuring ~34.5 ppm is recorded at ~8 cmbsf in the ambient sediment core 1-9A (Table 5). Shallow sediments throughout the global oceans display relatively higher level of NO_2^- relative to the deeper sediments, consistent with our findings (Codispoti et al., 2001; Engström et al., 2005; Gruber & Sarmiento, 1997). Microorganisms like nitrifiers readily consume O_2 in the shallow sediments to consecutively oxidize NO_2^- to NO_3^-, which produces relatively reduced NO_2^- and elevated NO_3^- concentrations in the shallow sediments (Christensen & Rowe, 1984; Vanderborght & Billen, 1975). However, core 13 alternatively displays higher NO_2^- concentrations that reach sediment depths of 600 cmbsf. One possibility for the elevated level of NO_2^- could be credited to core 13 being a hydrocarbon negative site located in the ambient sediments of the Scotian slope, unaffected by the presence of hydrocarbons, hence the NO_2^- has not been readily consumed by microorganisms yet. Some elevated NO_2^- concentrations can also be a function of greater level of denitrification being energetically favorable to the redox gradient of ocean floor surface sediments (Bowles & Joye, 2011). Another possibility for the elevated level of NO_2^- could be based on the assumption that the older cores might have experienced some NO_2^- disintegration into NO_3^- from sitting in the freezer for too long. Core 13 belongs to the site that was sampled in 2018, hence it hasn't been sitting in the freezer for as long as the cores that were sampled in 2015 and 2016 which make up all of the other deeper cores included in this study. Nitrate concentrations range from 0.3-50 ppm (Figure 6c) and on average also decrease with sediment depth. The highest concentration of NO_3^- in the deeper depths belongs to core 13 again ~13 ppm at 530 cmbsf. Being in the ambient sediment setting and having a higher concentration of NO_3^- at a greater depth could be explained using the same possibility as above being that as much NO_3^- hasn't been consumed by microorganisms yet. As discussed previously, in these ocean

floor surface sediments, microorganisms tend to turn to O_2 for energy first followed by NO_3^- and hence NO_2^-. Apart from their roles as EA's, the higher concentration of these anions in the deeper depths could be due to the slow consumption of these consequent EA's in the hydrocarbon negative sites coupled with their movement in the DNRA pathway. The first step in DNRA pathway usually involves the reduction of NO_3^- to NO_2^- through various microorganisms and the oxidation of NH_4^+ back to NO_3^- which in turn can increase their concentrations (GIBLIN et al., 2013; Joye & Anderson, 2008). Carbonate concentrations (Figure 6d) range between 0 – 1000 ppm and generally stay consistent with depth. Exceptions to this trend are two outliers between 200-300 cmbsf hosting the exceptionally high concentrations of CO_3^{2-} belonging to hydrocarbon positive site core 21. A lot of CO_3^{2-} gets stored as carbonate precipitates in the ocean floor sediments due to a wide range of geochemical processes and represents an immense pool of stored carbon in the marine carbon cycle (Gieskes et al., 2005). Sulfate concentrations (Figure 6e) range between 0–5000 ppm and on average decrease with sediment depth. Exceptions to this trend are some outliers highlighted with a red circle that dominantly belong to hydrocarbon negative cores. In hydrocarbon seep sites, some authigenic carbonates and SO_4^{2-} activities are largely controlled by biologically stimulated reactions and methane gas fluxes to the seafloor (Naehr et al., 2007). Dissimilatory sulfate reduction is one of the key processes causing low concentrations of SO_4^{2-} in the deeper marine benthic sediments (Jørgensen, 1982; Tarpgaard et al., 2011). Sulfate reducing bacteria are widely responsible for anerobic oxidation of organic matter and simultaneous SR until the SMTZ where methanogenesis takes over (Dale et al., 2008). In summary, the outliers for all of the anions seem unrelated to sediment depth or the presence/absence of hydrocarbons, indicating sample specificity or an interesting phenomena/microbial activity could be responsible for the unique behavior of these anions. As for the other anions, to find the approximate depth in our study where the NO_3^- -

NO_2^- reduction is occurring, site-specific studies were conducted for four different cores of the dataset. The rationale being these five cores had the best stratigraphic coverage with 6-9 different samples per core.

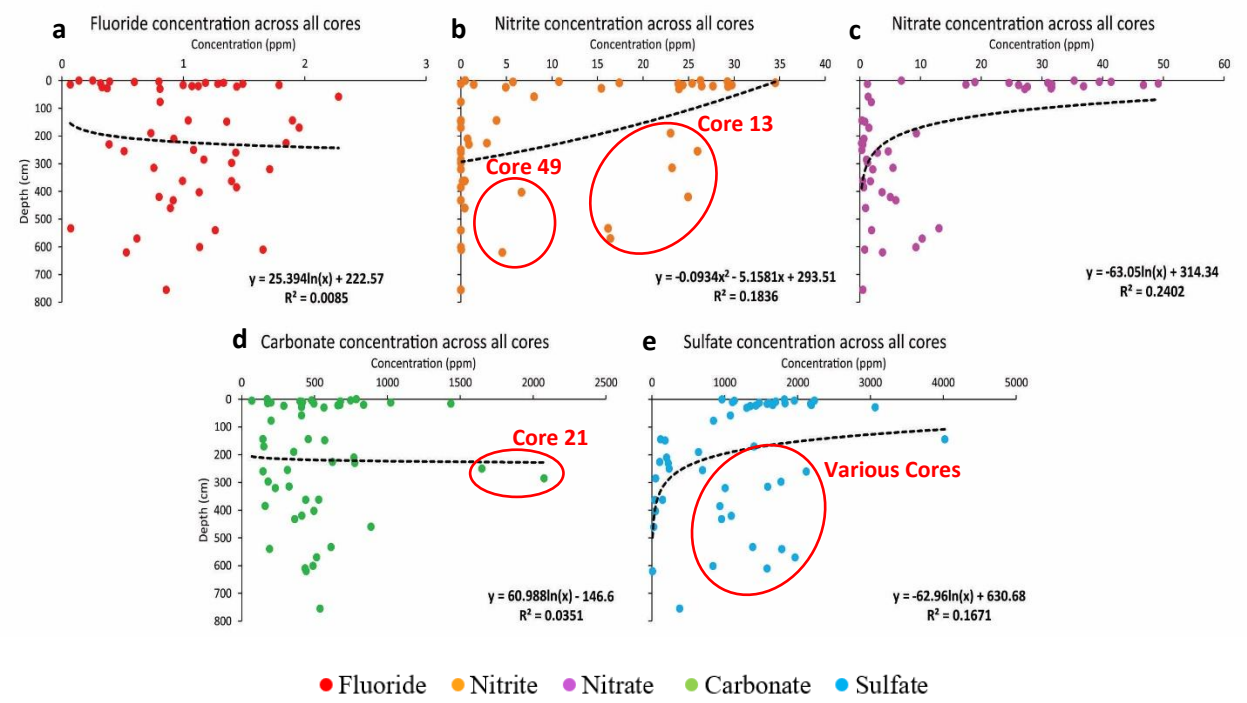

Figure 6 (a-e). Different anion concentrations (ppm) versus depth (cm). Red circles are representative of the outliers. Two of the red circles in the nitrite concentration are representing core 49 (hydrocarbon positive site) and core 13 (hydrocarbon negative site). The red circles represent the outliers for each anion concentrations and which core they belong to.

4.2.2. Site specific study

Two shallow push cores extending to 30 cmbsf and 7 deeper cores extending to 800 cmbsf were included in the PW anion dataset. Push cores 1-46 D and 1-9A were the selected shallow core sites while piston core 49 and gravity core 13 were the selected deeper core sites included for the site-

specific analysis with the aim to conduct a comparative study between two sites located inside the seep and the ambient sediment sites proximal to the two seeps (Figure 7 (a-e)).

4.2.2.1. Outside the seep

The sites outside the seep represent the ambient sediments of the Scotian slope, unaffected by presence of hydrocarbons in their vicinity. Core 1-9A (Figure 7a) and core 13 (Figure 7d) are shallow and deeper cores respectively, located outside the seep. Nitrate concentration ranges between 42–27 ppm, decreasing with sediment depth of 0–35 cmbsf in a consistent rise and fall pattern. Nitrite concentration ranges between 34–24 ppm, decreasing with sediment depth of 0–35 cmbsf in a similar rise and fall pattern. The two anions show no change between 0-5cm sediment depth. Typically, microorganisms tend to feed on O_2 in the ocean floor surface sediments as a source of nutrients, followed by which they tend to turn to the next best EA (NO_3^- and NO_2^-) after a decline in the availability of O2 with deeper sediments. Subsequently, the two anions present a cross cutting relationship after 10 cm depth. The cross-cutting relationship refers to the intervals where one anion is showing a surge, the other shows a parallel fall. This could be attributed to the cycling of nitrogen in marine sediments where microorganisms tend to feed on NO_3^- and produce NO_2^- as a result. Additionally, the regeneration of both the anions at different intervals could be ascribed to reasons like seawater diffusivity by bioturbation induced through the activities of surface dwelling organisms (Brimblecombe, 2014). For the deeper sediments, concentration is comparatively reduced (notice the change in scale). Nitrate concentration is ranging from 19–10 ppm, decreasing with sediment depth of 0–600 cmbsf in a similar rise and fall pattern with much less variability. Nitrite concentration is ranging from 6–15 ppm, increasing with sediment depth of 0–600 cmbsf in a similar rise and fall pattern with much less variability. Also, the cross-cutting

relationship which was noticed in the shallow sediments is replicated at ~30 cmbsf even in the deeper sediments. Carbonate concentration, between the shallow 0–35 cmbsf ranges from 1500–560 ppm and stays quite consistent with depth, aside from an exceptionally high surge in concentration between 10–20cm. For the deeper sediments, between 0-600 cmbsf, the concentration of CO_3^{2-} is comparatively reduced (notice the change in scale). Carbonate concentration ranges from 500–100 ppm and seems macroscopically less affected with depth for the deeper sediments between 0–600 cmbsf. Sulfate concentration, between the shallow 0-35 cmbsf ranges from 2200–1400 ppm and is decreasing with depth, aside from two exceptionally high surge in concentration between 0–5 and 10–20 cmbsf. The rapid surge between 10–20cm is parallel and analogous to the surge in CO_3^{2-} and NO_2^- and a decline in NO_3^- at the same depth steering to perhaps a common process occurring at this specific depth, for example, a result of reduced microbial activity. In anoxic sediment zones of the global oceans, anions tend to exhibit similar gradients with respect to each other and with respect to the depth. In these anoxic zones, NO_2^- and microbial abundance is usually elevated while NO_3^- abundance is depleted (Ulloa et al., 2012). In highly eutrophic anoxic conditions, sulfide oxidizing bacteria tend to detoxify sulfide and reduce NO_3^- (Callbeck et al., 2021). Porewater sulfide is part of a rather dynamic system of the sulfur cycle in ocean floor surface sediments (Rickard, 2012). In these anoxic zones, a large SO_4^{2-} pool tends to accumulate and support assimilatory sulfate reduction (ASR) and hold a potential to span the wide range of detox conditions (Jørgensen et al., 2019; Wasmund et al., 2017). With the reduced NO_3^- and enriched NO_2^-, CO_3^{2-} and SO_4^{2-} in our data, it seems like the region between 10-20cm could perhaps be attributed to reduced microbial activity and a common process like a zone of anoxia causing the rapid surge in concentrations.

4.2.2.2. Inside the seep

The sediments inside the seep are representative of conditions where the sediments and the PW have been altered due to the presence of hydrocarbons. Figure 7b and 7c represent the shallow and the deeper anion concentration behavior for ambient sediments located inside these cold seep sites. Between 0–30 cmbsf, the concentration of NO_3^- ranges between 50–7 ppm with a gradual increase with depth. Nitrite concentration ranges between 25–0 ppm and shows a similar varying and increasing trend from 0–35 cmbsf. Although the two anions do not show the cross-cutting relationship noticed for anion gradients in an ambient setting, they show a consistent rise and fall pattern of for all the anions in a very similar gradient variation. For the deeper sediments, between 70–700 cmbsf, the concentration of these anions is quite low (notice the change in scale). Nitrate concentration ranges between 3.5–0.2 ppm and shows a similar varying and increasing trend from 0-600 cmbsf. Nitrite concentration ranges between 6.5–0 ppm and displays a similar varying and increasing trend from 0–600 cmbsf. The two anions show similar gradient variation attributing to perhaps a common microbially mediated process occurring through each interval. Carbonate concentration ranges between 900–200 ppm and displays a similar varying and increasing trend from 0–600 cmbsf. Sulfate concentration ranges between 1600-0 ppm and displays a sharp declination in trend from 0–600 cmbsf. Interestingly, unlike the trend of SO_4^{2-} increasing with depth for the ambient sediments (Figure 7b) in these hydrocarbon rich sediments, sulfate goes to total exhaustion by 500–600 cmbsf. In these cold seep, hydrocarbon positive sites, the processes that guide the biogeochemistry of this region is mostly attributed to AOM and SR. Generally, the trend seems to be that the CO_3^{2-} concentration seems macroscopically less affected than the other anions in terms of concentration as well as variation similar to how it seemed outside the seep, in the ambient sediments. To oversimplify the variation happening through each interval, in terms of

each anion, an in-depth specific interval-based study would be required in the future to insinuate anything concrete. Although generally, previous studies (Joye et al., 2004) also show that concentration of SO_4^{2-} and H2S is usually high and variable in and around seep sites, consistent with our findings. The possibility to explain the complete exhaustion of SO_4^{2-} in these hydrocarbon rich sediments, could be that AOM and SR being the two dominant processes, pose a very strong underlying effect and total exhaustion of SO_4^{2-} is occurring due to methanogenesis and AOM. In these cold seep sites, microorganisms sufficiently have more energy due to the presence of hydrocarbons and readily deplete the available EA's and completely exhaust them within 600 cmbsf. A syntrophic close relationship between the methane oxidizing and sulfate reducing microorganisms acts as the key intermediaries for AOM (Hoehler et al., 1994, 2001). A large pool of anaerobic methanotrophs within the anoxic sediments consume the methane fluxing from cold seep reservoirs and partake in higher rates of SR (Joye et al., 2004). It is also a common occurrence to have exceedingly higher rates of SR and AOM in the deep marine benthic sediments of cold seep habitats (Lin & Morse, 1991). To confirm this speculation in our data, a comparative study of the ambient marine benthic sediments and hydrocarbon positive sites was prepared.

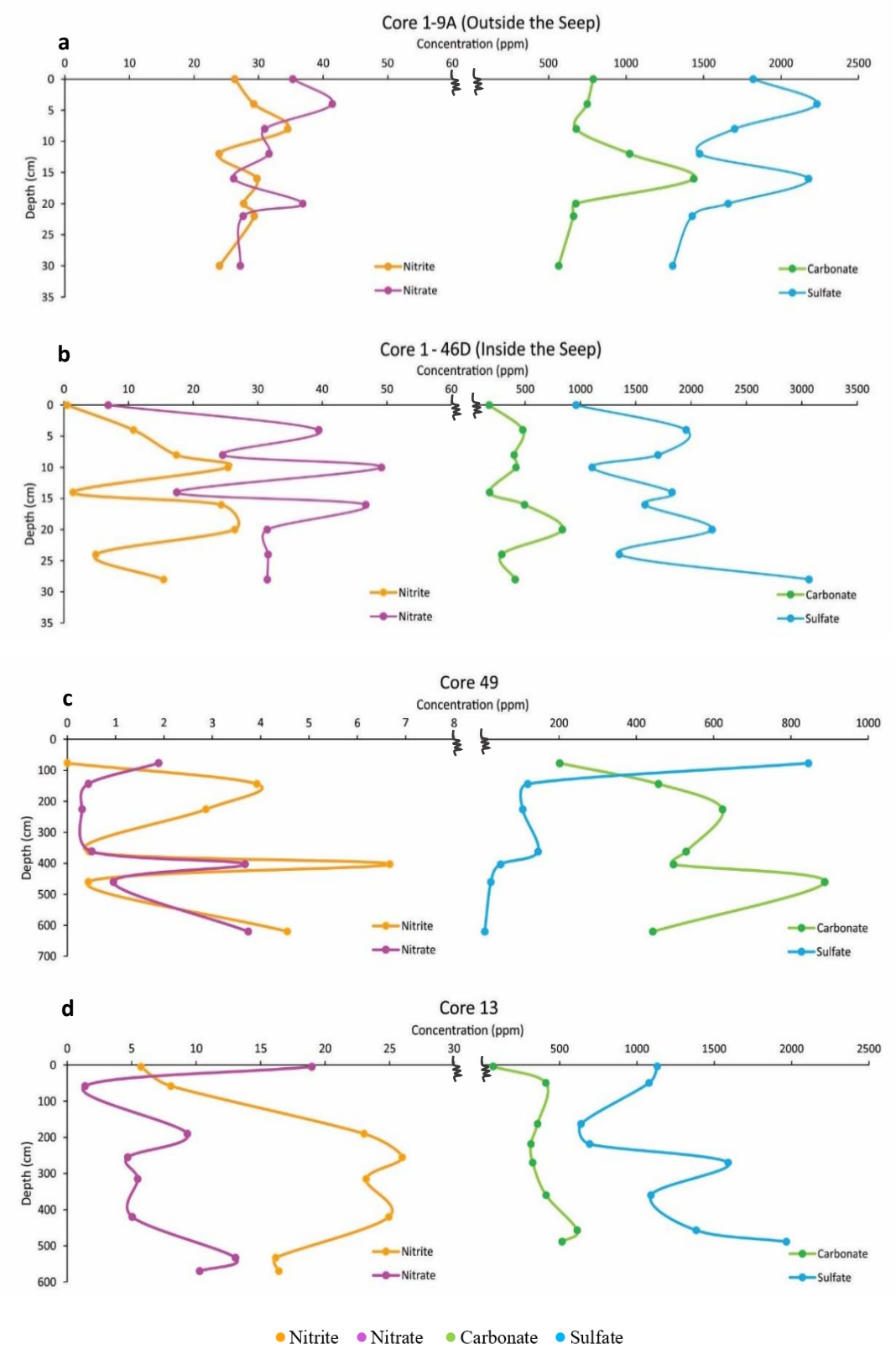

Figure 7 (a-d). Depth profiles of anions detected across various cores. Note the varying concentration scale for each core.

4.3. Comparative study of ambient marine benthic sediments to hydrocarbon impacted sediments

Nutrients provide essential energy for microorganisms to flourish. The anions in the ocean floor surface sediments behave as essential nutrients for microorganisms and are continuously undergoing biodegradation and remineralization. The addition of hydrocarbon seepage at the Scotian Slope provides an extra push to the system as the hydrocarbons provide extra nutrients and energy to the system to correctly consume more organic matter. As discussed previously, AOM coupled with SR are the two major processes that drive most of the processes in seep sediments (Orcutt et al., 2010) . Various studies show that increased sulfate reduction can be directly linked to an increased presence of hydrocarbons, sometimes in magnitudes of two times higher (Grant et al., 1998; Orcutt et al., 2010 Dong et al., 2020). Sulfate reducing bacteria are common microorganisms in these anoxic environments and their activity level is directly related to the presence of more nutrients. The basic hierarchy that anions follow as EA's is after the consumption of O_2 in the shallow sediments, NO_3^- gets exhausted first, followed by NO_2^-, followed by SO_4^{2-}, and then CO_2 and this pattern can be reconstructed using the anion profiles. Figure 8 (a-e) is representative of the standard addition data for the samples in this study divided by their hydrocarbon positive (green) or hydrocarbon negative (black) behavior.

4.3.1. Nitrate and Nitrite Recycling

In marine sediments, especially at cold seeps, NO_3^- and NO_2^- are of minor importance relative to AOM and SR processes because their abundance is minimal and harder to quantify compared to SO_4^{2-} (Ruff, 2020). Hydrocarbon negative refers to the ambient sediments of the Scotian Slope.

Nitrite concentration (Figure 8b) of the ambient sediments shows a shift towards a lower concentration for the shallow sediments with a poor coefficient of determination ($R^2 = 0.36$) while the hydrocarbon positive sites show a similar trend but at a much higher concentration at a greater depth with $R^2 = 0.28$. Nitrate concentration (Figure 8c) with depth shows a similar pattern for both hydrocarbon positive $R^2 = 0.29$ and negative sites $R^2 = 0.42$. While NO_3^- concentration in shallow sediments is almost equal, there is a greater difference in concentration occurring at a deeper depth. Unlike the other anions displaying cross comparative trends, it appears that the NO_3^- and NO_2^- concentration has been shifted to a shallower depth. In cold seep surface sediments, microbial activity is much higher in hydrocarbon positive sites than in the ambient sediments due to the presence of hydrocarbons providing the additional nutrients and energy (Orcutt et al., 2010). In these environments, SRB and certain denitrifying bacteria hold a analogous metabolic capacity to degrade a greater quantity of liquid hydrocarbons (Widdel & Rabus, 2001). These denitrifying bacteria preferentially exhaust NO_3^- and NO_2^- as their first EA's. Studies like (M. Bowles & Joye, 2011; Joye et al., 2004) substantiate their individual PW profiles with significant rates of heterotrophic potential denitrification and NO_3^- being depleted rapidly in the surface sediments of cold seep sites. Since the microorganisms essentially have more nutrients and energy from those hydrocarbons, they tend to exhaust a greater quantity of these anions. Figure 8b and 8c show good representation of this phenomena as it is noticeable that there is less NO_3^- and NO_2^- concentration in the hydrocarbon rich sediments compared to the ambient sediments. Essentially, the increase in microbial activity has caused more exhaustion of these EA's in the shallower depths itself. Additionally, the PW data displays the difference in the trendlines of NO_2^- being much farther away than the difference in the trendlines of NO_3^- (Figure 8b and c respectively). This difference could indicate greater NO_2^- removal suggesting additional processes such as assimilation, DNRA,

or NO_2^- production coupled with removal via ANAMMOX prominently occurring in the sediments of the Scotian Slope, just to name a few (M. Bowles & Joye, 2011).

4.3.2. Sulfate Reduction

Sulfate is the next best EA that microorganisms tend to exhaust in marine habitats after the exhaustion of NO_3^- and NO_2^- . Since SO_4^{2-} reduction is usually a coupled process with AOM in cold seep sediments, the majority of microorganisms tend to be methane dominant in these environments (Treude et al., 2014). The reduction of EA's in these environments tend to be dependent on AOM + ANME with a reverse methanogenesis bacterial syntropy pathway (Orcutt et al., 2010). In cold seep sediments of the world, hydrocarbon presence is directly proportional to SO_4^{2-} reduction. In previous studies of the Scotian Slope, it has been suggested that SO_4^{2-} reduction accounts for a major pathway for carbon mineralization and this area is quite similar to a study conducted at the Gulf of Maine with ~55% of the system being dependent on the high quantity of SO_4^{2-} in the region (Hines et al., 1991; Grant et al., 1998). Sulfate concentration (Figure 8e) with depth, in the shallow sites, both hydrocarbon positive and negative commence at a similar concentration ranging between 1000–2000 ppm but after 100 cmbsf, there is variable shifts in concentration. While the hydrocarbon positive sites reduce to a range between 0–50 ppm and the trendline presents a shift towards a shallower depth, the ambient sediments still stay between 1000–2000 ppm concentration range even at the deeper depths. Implying greater SO_4^{2-} reduction has occurred at shallower depths in hydrocarbon influenced sediments while as much sulfate reduction hasn't yet transpired with the ambient sediments at the same depth, also corroborating with the results discussed previously.

4.3.3. Carbonate Variation

The anthropogenic CO_2 released to the atmosphere tends to accumulate in the ocean floor surface sediments as burial CO_3^{2-} (Archer, 1996; Keil, 2017). Anaerobic oxidation of methane in cold seep sites causes an increase in alkalinity, hence impacts increased formation of CO_3^{2-} from the metabolic activities of methane reducing microorganisms and being confined to anoxic environments (Aloisi et al., 2000; Peckmann et al., 2001; Valentine, 2002). Carbonate rocks serve as an important tool to track the relationships of ancient seep structures that accommodate presence of gas hydrates (Peckmann & Thiel, 2004). Depth coupled with alkalinity of sediments is also an important factor for CO_3^{2-} cycling and preservation (Morse & Mackenzie, 1990). The precipitation rate these carbonate rocks generally is highest near the sediment water interface and gradually reduces (Han et al., 2004; Karaca et al., 2010). The PW profile of CO_3^{2-} concentrations demonstrates a similar variability between ambient and hydrocarbon influenced sediments (Figure 8d). Both trendlines hold exceptionally low correlations (R^2=0.02 and R^2=0.01, respectively) suggesting that the CO_3^{2-} depth trend is not subject to a massive change. It is possible that the steady concentration of CO_3^{2-} with depth of 900 cmbsf suggests that most of the CO_3^{2-} might be present in the form of aggregates in the ocean floor surface sediments and hence the PW profile doesn't show much variation according to depth. In cold seep sites, CO_3^{2-} precipitation formed aggregates are a common occurrence and an important indication of seafloor gas venting and existence of shallow gas hydrates (Wang et al., 2014). Granting there isn't much change in concentration range between the hydrocarbon positive and the ambient sediments, it probably signifies slow consumption of the anion by sulfate reducing microorganisms.

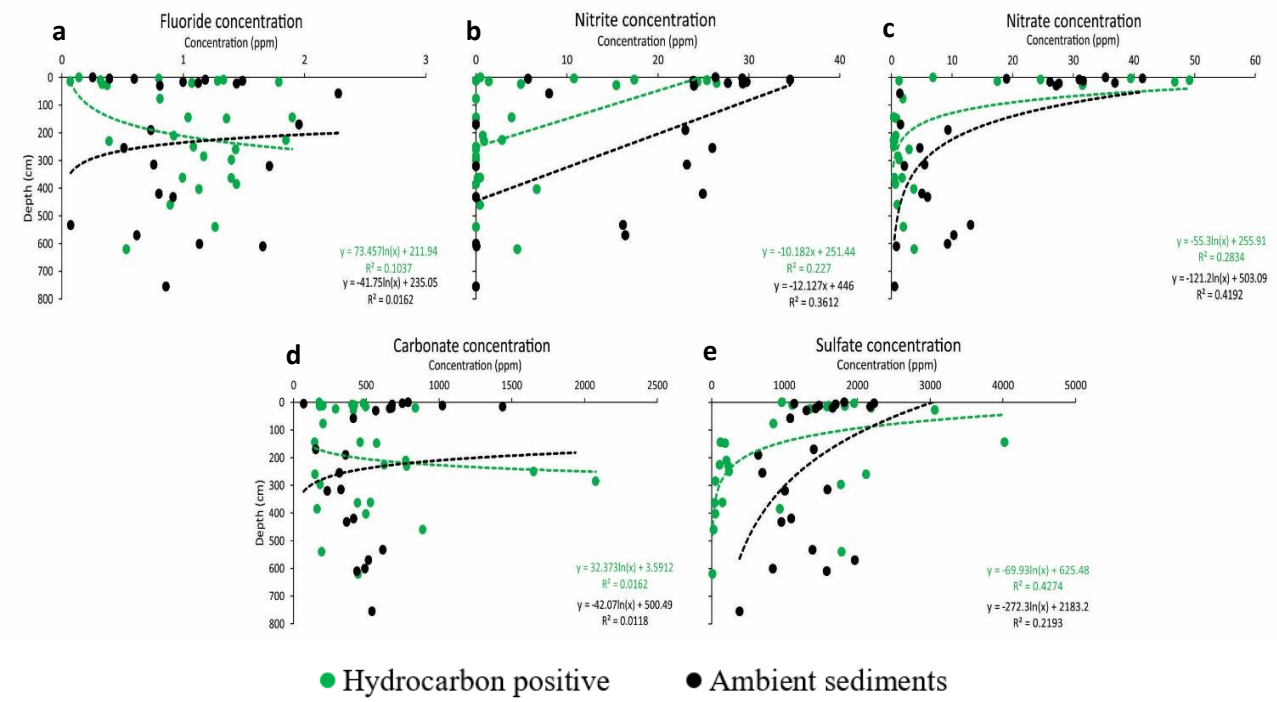

Figure 8 (a-e). Different anion concentrations (ppm) v/s depth (cmbsf) divided for hydrocarbon positive cores (green) v/s hydrocarbon negative cores (black).

5. Conclusions

The internal calibration method of standard addition proved to be better than the external calibration method of calibration curve to measure the anion PW concentrations of unknown samples with complex matrices and an unknown range of varying concentrations. The outliers for the anions seem unrelated to sediment depth or the presence/absence of hydrocarbons, indicating the outliers being possibly dependent on sample specificity or interesting phenomena/microbial activity pertaining to the unique site. The site-specific analysis indicates cross-cutting relationship (i.e., increase in one anion correlates with decrease in the other anion and vice versa) for NO_3^- and NO_2^- in the ambient marine benthic sediments, while a consistent rise and fall in the concentration of PW anions in the presence of hydrocarbons. Carbonate concentration seems unrelated to the

presence or absence of hydrocarbons. Sulfate concentration decreases dramatically in both ambient and hydrocarbon impacted marine benthic sediments although, in hydrocarbon impacted sites, SO_4^{2-} reduction appears to occur at a much shallower depth suggesting that the redox gradient is much more pronounced. Nitrate and NO_2^- trends show similar reduction patterns occurring at shallower depths for hydrocarbon positive sediments. Usually in benthic marine sediments, widescale microbial and bacterial activity causes the consumption of anions and EA's whereas in hydrocarbon impacted sediments, hydrocarbons provide the extra guiding force for faster consumption of these anions. Methane-dependent SR is mediated by microorganisms like methanotrophic archaea in cold seeps (Orcutt et al., 2010). The redox gradient produced by these SRB and SRM in the Scotian Slope display a similar, higher rate of NO_3^-, NO_2^- and SO_4^{2-} reduction in hydrocarbon impacted sediments causing the shift in reduction appearing at a shallower depth.

6. Appendix

6.1. Appendix A

Table A1. Abbreviations used and what they represent.

Abbreviations	Representing
F–	Fluoride
NO_3^-	Nitrate
NO_2^-	Nitrite
CO_3^{2-}	Carbonate
SO_4^{2-}	Sulfate
SO_3^{2-}	Sulfite
PO_4^{3-}	Phosphate
S^{2-}	Sulfide
O_2	Oxygen

CO_2	Carbon Dioxide
IC	Ion Chromatography
PW	Porewater
cmbsf	centimeters below seafloor
GEOSEC	Geochemical Ocean Sections
SR	Sulfate Reduction
AOM	Anaerobic Oxidation of Methane
EA	Electron Acceptor
SMTZ	Sulfate Methane Transition Zone
SRB	Sulfate Reducing Bacteria
SRM	Sulfate Reducing Microorganisms
ASR	Assimilatory Sulfate Reduction
DSR	Dissimilatory Sulfate Reduction
DNRA	Dissimilatory Nitrate Reduction to Ammonia
DOC	Dissolved Organic Carbon
POC	Particulate Organic Carbon

Table A2: Standard addition dilution each sample was subject to with sample collection year, core number, and depth.

Year	Core	Archived Sample Name	Depth (cm)	Standard Concentration (ppm) (S+D - SO32- - CO32-)	PW (10 times diluted) + concentration standard				
					PW + 0ppm	PW + 2ppm	PW + 5ppm	PW + 10ppm	PW + 20ppm
2015	9	NSPC 2015018-0009 S01 B 144-149cm	144	20-20-200	✓		✓		
		NSPC 2015018-0009 S03 B 297-302cm	297	20-20-200	✓		✓		
		NSPC 2015018-0009 S04 B 363-369cm	363	20-20-200	✓		✓		
2016	21	2016011-021 S01 B 12-17cm	77	20-20-100	✓	✓	✓	✓	
		2016011-021 S02 B 148-155cm	144	20-20-100	✓	✓	✓	✓	

		2016011-021 S03 B 210-215cm	226	20-20-100	✓	✓	✓	✓	
		2016011-021 S04 B 230-236cm	362	20-20-100	✓	✓	✓	✓	
		2016011-021 S05 B 250-255cm	403	20-20-100	✓	✓	✓	✓	
		2016011-021 S06 B 285-290cm	460	20-20-100	✓	✓	✓	✓	
	49	2016011-049 S01 B 77-82cm	620	20-20-100	✓	✓	✓	✓	
		2016011-049 S02 B 144-149cm	12	20-20-100	✓	✓	✓	✓	
		2016011-049 S03 B 226-231cm	148	20-20-100	✓	✓	✓	✓	
		2016011-049 S04 B 362-367m	210	20-20-100	✓	✓	✓	✓	
		2016011-049 S05 B 403-409cm	230	20-20-100	✓	✓	✓	✓	
		2016011-049 S07 B 460-465cm	250	20-20-100	✓	✓	✓	✓	
		2016011-049 S08 B 620-625cm	285	20-20-100	✓	✓	✓	✓	
	32	2016011-032 S01 B 260-265cm	260	20-0-200	✓		✓		
		2016011-032 S02 B 385-390cm	385	20-0-200	✓		✓		
		2016011-032 S03 B 540-545cm	540	20-0-200	✓		✓		
	33	2016011-033 S01 B 170-175cm	170	20-0-200	✓		✓		
		2016011-033 S02 B 320-325cm	320	20-0-200	✓		✓		
		2016011-033 S03 B 610-615cm	610	20-0-200	✓		✓		
	44	2016011-044 S01 B 432-437m	432	20-0-200	✓		✓	✓	
		2016011-044 S02 B 601-606cm	601	20-0-200	✓		✓	✓	
		2016011-044 S03 B 755-760cm	755	20-0-200	✓		✓	✓	
2018	13	2018041-0013 gc 5-15cm	5	20-0-200	✓		✓	✓	
		2018041-0013 gc 58-62 cm	58	20-0-200	✓		✓	✓	
		2018041-0013 gc 190-195cm	190	20-0-200	✓		✓	✓	
		2018041-0013 gc 255-260cm	255	20-0-200	✓		✓	✓	
		2018041-0013 gc 315-320 cm	315	20-0-200	✓		✓	✓	
		2018041-0013 gc 420-425cm	420	20-0-200	✓		✓	✓	
		2018041-0013 gc 533-538cm	533	20-0-200	✓		✓	✓	
		2018041-0013 gc 570-575cm	570	20-0-200	✓		✓	✓	
2021	1-46 D	46D 0-2cm	0	50-0-500	✓		✓	✓	✓
		46D 4-6cm	4	50-0-500	✓		✓	✓	✓
		46D 8-10cm	8	50-0-500	✓		✓	✓	✓
		46D 10-12cm	10	50-0-500	✓		✓	✓	✓
		46D 14-16cm	14	50-0-500	✓		✓	✓	✓
		46D 16-18cm	16	50-0-500	✓		✓	✓	✓
		46D 20-22cm	20	50-0-500	✓		✓	✓	✓
		46D 24-26cm	24	50-0-500	✓		✓	✓	✓
		46D 28-30cm	28	50-0-500	✓		✓	✓	✓
	1-9A	9A 0-2 cm	0	50-0-500	✓		✓	✓	✓
		9A 4-6cm	4	50-0-500	✓		✓	✓	✓
		9A 8-10cm	8	50-0-500	✓		✓	✓	✓

9A 12-14cm	12	50-0-500	✓	✓	✓	✓
9A 16-18cm	16	50-0-500	✓	✓	✓	✓
9A 20-22cm	20	50-0-500	✓	✓	✓	✓
9A 22-26cm	22	50-0-500	✓	✓	✓	✓
9A 30-34cm	30	50-0-500	✓	✓	✓	✓

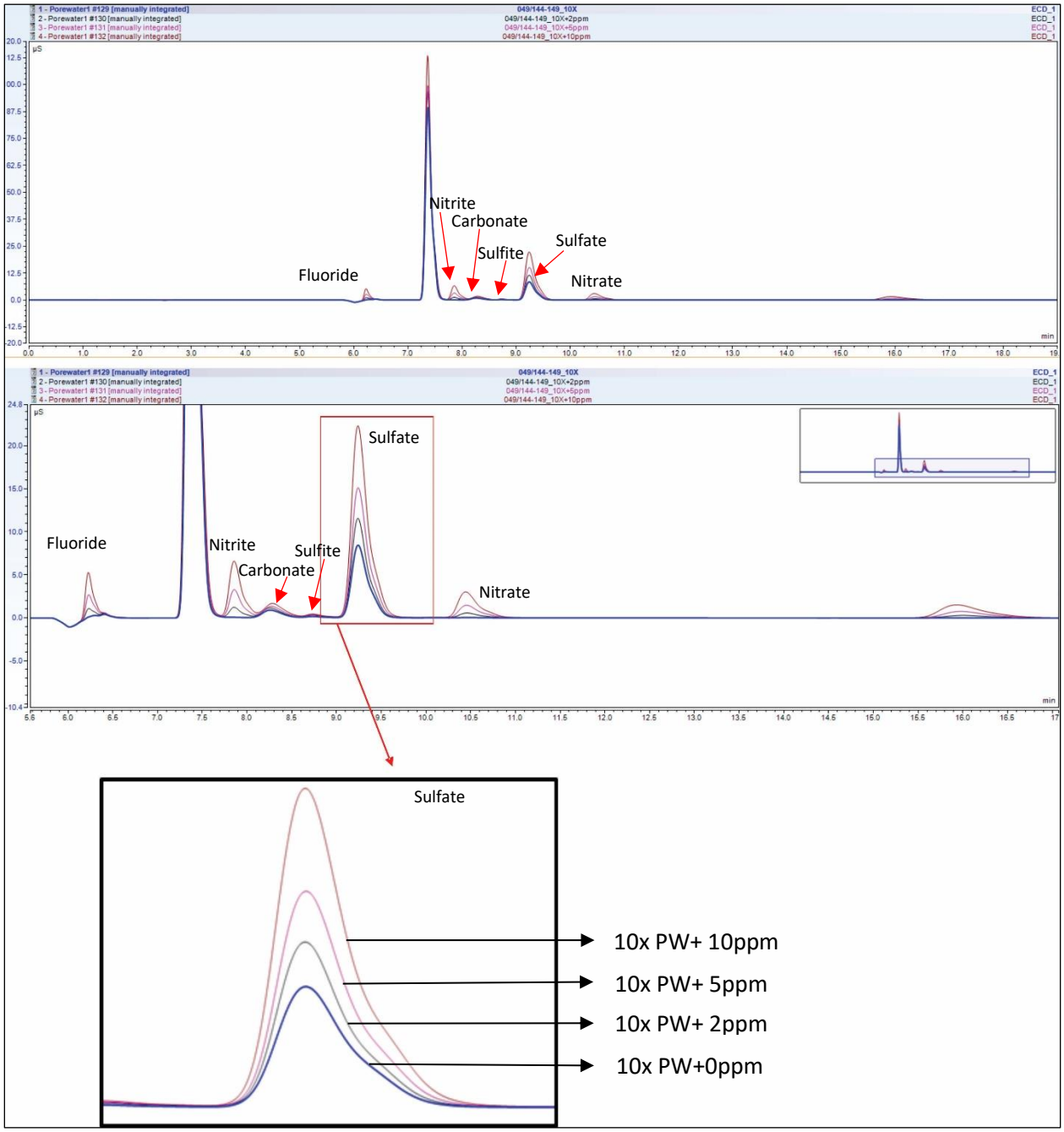

Figure A1. Example chromatogram recorded for different anion concentrations of 10 times diluted PW + quantity of standard addition dilution. (example Core 49 144-149cm)

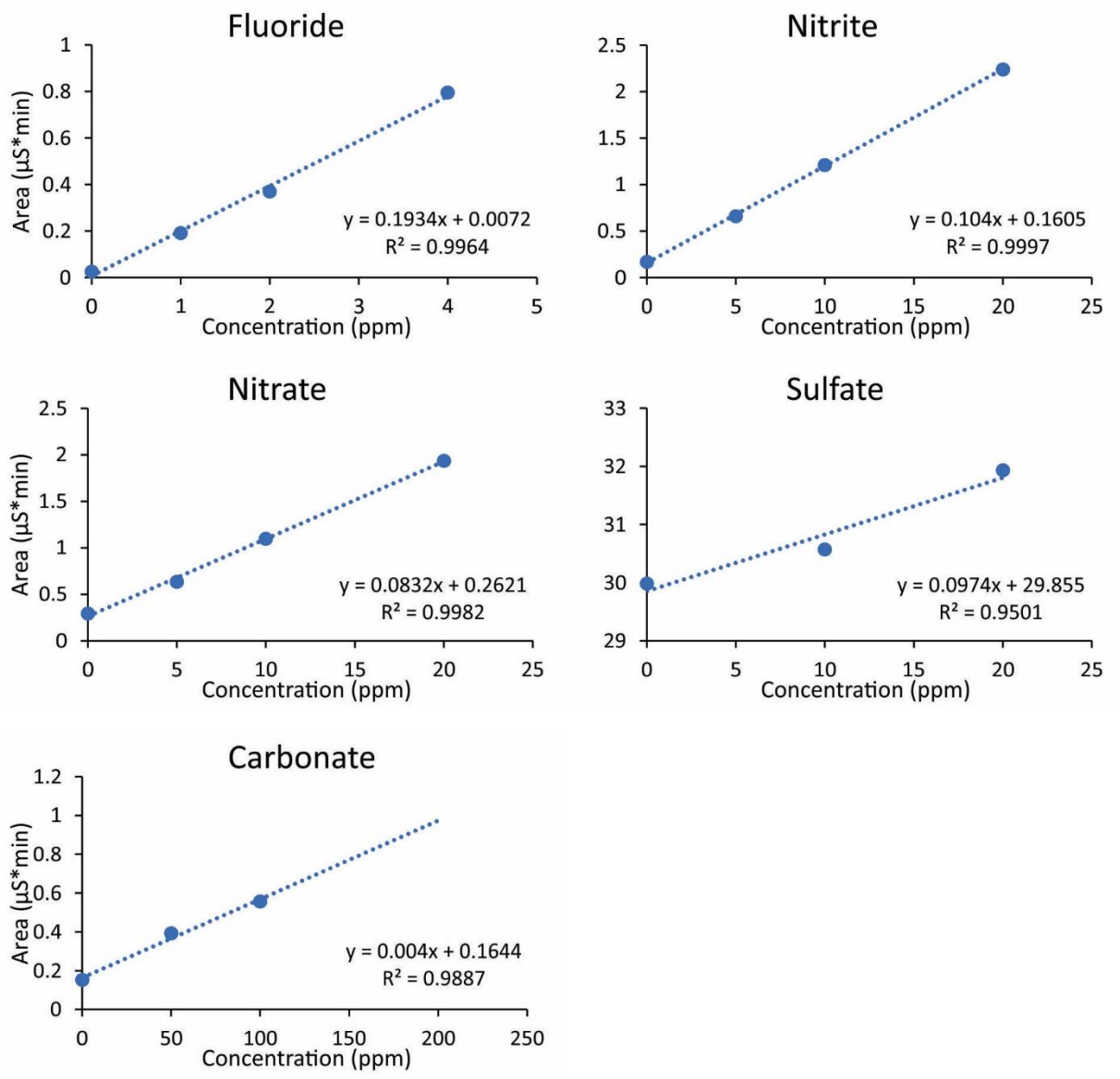

Figure A2. Example of standard addition dilution regression curves that were created for each sample to resolve matrix effects. (example Core 1-46D 28-30cm)

6.2. Appendix B

Table B1. Variance Percentage calculation table between standard addition and calibration curve data.

Variance % Calculation									
Year	Core	Depth		Difference between standard addition and calibration curve					
		Range	Exact	Fluoride	Nitrite	Carbonate	Sulfite	Sulfate	Nitrate
2015	Core 9	144-149 cm	144	-0.3	-2.5	2.5	0	2645.6	-2.9
		297-302 cm	297	-0.3	-2.5	2.4	0	1075.0	-3.1
		363-369 cm	363	-0.4	-2.5	-38.7	0	16.7	-3.1
2016	Core 49	77-82 cm	77	-1.0	-2.5	7.8	0	-505.4	-1.3
		144-149 cm	144	-0.8	-1.5	-187.9	0	33.5	-2.8
		226- 232 cm	226	0.5	-1.2	-43.2	0	40.6	-2.9
		362- 367 cm	362	-0.9	-3.0	-158.8	0	56.2	-5.5
		403-409 cm	403	-0.8	-3.1	-70.1	0	19.9	0.4
		460-465 cm	460	-1.0	-3.6	386.9	0	6.5	-2.3
		620- 625cm	620	-1.0	-4.0	67.0	0	0.1	0.5
	Core 21	12-17 cm	12	-0.4	-2.5	-13.5	0	457.2	-2.0
		148-155 cm	148	-1.2	-2.5	19.2	0	53.4	-2.4
		210-215 cm	210	-0.9	-2.4	191.7	0	75.2	-4.1
		230-236 cm	230	-0.8	-3.7	206.8	0	86.9	-4.9
		250-255 cm	250	-0.8	-2.5	1023.4	0	124.0	-2.9
		285-290 cm	285	-1.1	-2.5	1362.4	0	17.0	-2.1
	Core 32	260-265 cm	260	-0.3	-2.5	-9.7	0	650.3	-0.3
		385-390 cm	385	-0.3	-2.5	-13.6	0	-435.7	-2.6
		540-545 cm	540	-0.4	-2.5	-14.6	0	461.5	-1.3

	Core 33	170-175 cm	170	0.1	-2.5	13.3	0	-43.5	-1.7
		320-325 cm	320	-0.2	-2.5	31.6	0	-343.4	-1.6
		610-615 cm	610	-0.2	-2.5	101.3	0	535.8	-3.2
	Core 44	432-437 cm	432	-0.9	-2.5	-1.8	0	94.4	2.7
		601-606 cm	601	-0.6	-2.5	9.2	0	277.5	6.0
		755-760 cm	755	-0.8	-2.5	18.5	0	45.2	-5.0
2018	Core 13	5-15cm	5	-0.8	-4.0	17.9	0	-113.9	-0.1
		58-62cm	58	-0.5	-2.5	174.3	0	-194.7	-2.8
		190-195cm	190	-0.6	2.0	170.4	0	-493.2	-4.5
		255-260cm	255	-0.8	0.0	10.5	0	-554.0	-1.9
		315-320cm	315	-0.7	-0.8	31.1	0	448.2	-1.9
		420-425cm	420	-0.7	-1.5	19.4	0	90.7	-1.6
		533-538cm	533	-1.0	-1.9	229.2	0	586.3	-1.9
		570-575cm	570	-0.6	-1.9	129.2	0	1233.7	-3.9
2021	Core 1-46D	0-2cm	0	-1.6	-3.7	-7.3	0	-349.8	-11.1
		4-6cm	4	-1.2	-1.4	346.4	0	520.7	-10.0
		8-10cm	8	-0.7	-6.1	290.6	0	140.0	-4.8
		10-12cm	10	-1.4	-4.6	-85.1	0	-347.1	-8.7
		14-16cm	14	-1.6	-5.4	-48.8	0	320.1	-11.2
		16-18cm	16	-0.1	-4.3	90.6	0	1.9	-10.8
		20-22cm	20	-1.1	-8.9	117.3	0	574.6	-10.5
		24-26cm	24	-1.2	-6.0	4.9	0	-92.5	-13.4
		28-30cm	28	-1.3	-2.6	-165.0	0	1686.8	-7.0
	Core 1-9A	0-2cm	0	-1.8	-8.1	93.9	0	319.9	-9.0
		4-6cm	4	-1.4	-5.1	56.4	0	700.6	-6.5

8-10cm	8	-1.3	-8.0	24.1	0	193.4	-15.8
12-14cm	12	-0.9	-3.9	76.1	0	-61.3	-11.1
16-18cm	16	-1.4	-6.9	333.0	0	639.6	-6.9
20-22cm	20	-1.2	-8.7	-87.2	0	151.8	-12.1
22-26cm	22	-1.2	-10.1	12.3	0	-65.6	-11.1
30-34cm	30	-1.1	-7.6	58.4	0	-202.1	-7.3
Average		-0.8	-3.5	95.7	0	211.6	-4.7
Standard Deviation		0.5	2.4	259.3	0	559.7	4.4
%age Variance		-44.8	-25.6	22.1	0	21.5	-26.5

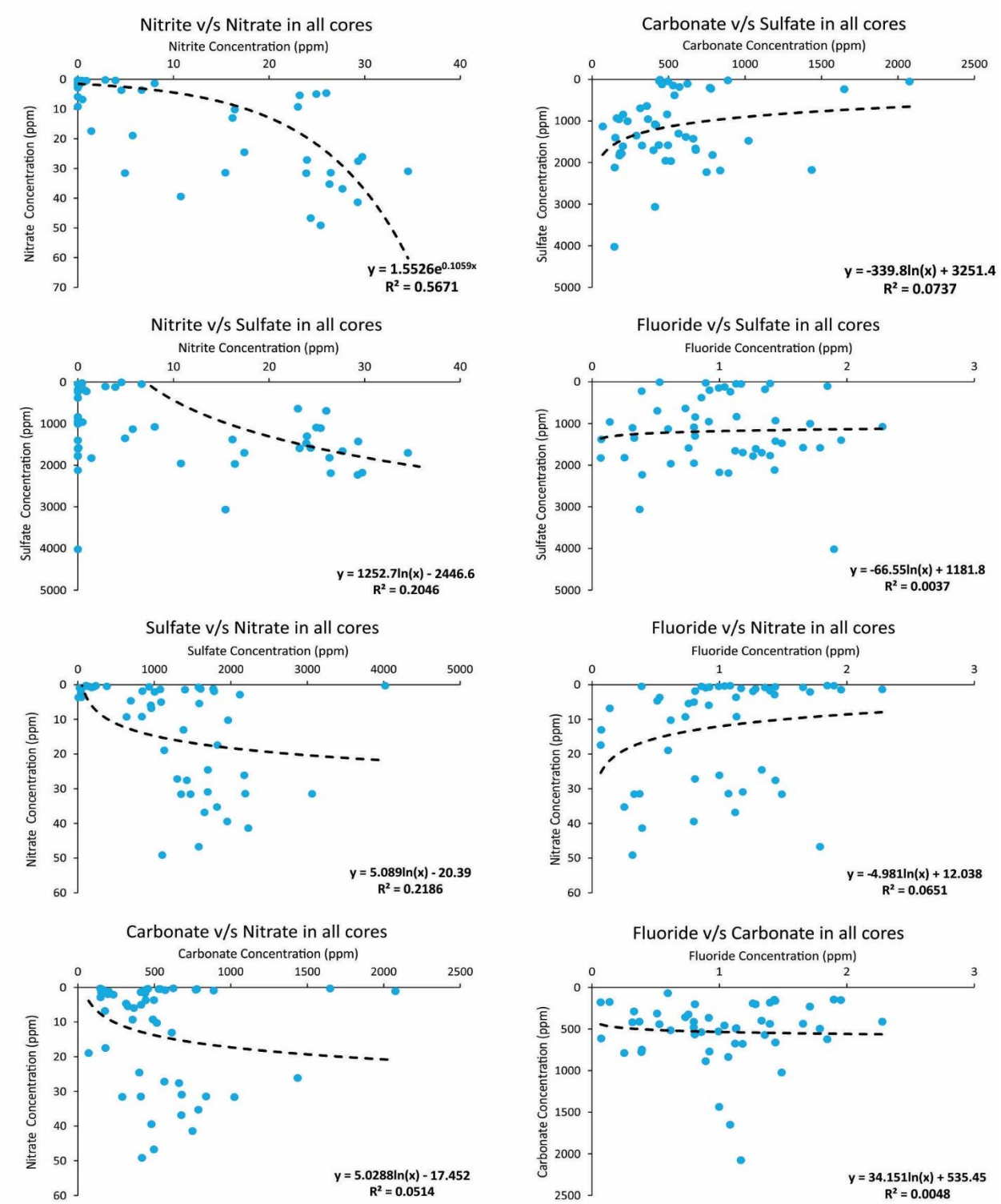

Figure B1: Cross plots of anion concentrations (ppm) based on the standard addition method.

7. List of References

Adams, M. M., Hoarfrost, A. L., Bose, A., Joye, S. B., & Girguis, P. R. (2013). Anaerobic oxidation of short-chain alkanes in hydrothermal sediments: Potential influences on sulfur cycling and microbial diversity. *Frontiers in Microbiology*, *4*, 110. https://doi.org/10.3389/fmicb.2013.00110

Aharon, P., & Fu, B. (2000). Microbial sulfate reduction rates and sulfur and oxygen isotope fractionations at oil and gas seeps in deepwater Gulf of Mexico. *Geochimica et Cosmochimica Acta*, *64*(2), 233–246. https://doi.org/10.1016/S0016-7037(99)00292-6

Aloisi, G., Pierre, C., Rouchy, J.-M., Foucher, J.-P., & Woodside, J. (2000). Methane-related authigenic carbonates of eastern Mediterranean Sea mud volcanoes and their possible relation to gas hydrate destabilisation. *Earth and Planetary Science Letters*, *184*(1), 321–338. https://doi.org/10.1016/S0012-821X(00)00322-8

Andersen, J. E. T. (2017). The standard addition method revisited. *TrAC Trends in Analytical Chemistry*, *89*, 21–33. https://doi.org/10.1016/j.trac.2016.12.013

Archer, D. E. (1996). An atlas of the distribution of calcium carbonate in sediments of the deep sea. *Global Biogeochemical Cycles*, *10*(1), 159–174. https://doi.org/10.1029/95GB03016

Avdalovic, N., & Liu, Y. (2021). Chapter 12—Capillary ion chromatography. In C. Pohl, N. Avdalovic, & K. Srinivasan (Eds.), *Separation Science and Technology* (Vol. 13, pp. 303–322). Academic Press. https://doi.org/10.1016/B978-0-12-813075-9.00015-7

Bader, M. (1980). A systematic approach to standard addition methods in instrumental analysis. *Journal of Chemical Education*, *57*(10), 703. https://doi.org/10.1021/ed057p703

Barge, L. M., Flores, E., Baum, M. M., VanderVelde, D. G., & Russell, M. J. (2019). Redox and pH gradients drive amino acid synthesis in iron oxyhydroxide mineral systems.

Proceedings of the National Academy of Sciences, *116*(11), 4828–4833. https://doi.org/10.1073/pnas.1812098116

Baturin, G. N. (2003). Phosphorus Cycle in the Ocean. *Lithology and Mineral Resources*, *38*(2), 101–119. https://doi.org/10.1023/A:1023499908601

Blouet, J.-P., Imbert, P., & Foubert, A. (2017). Mechanisms of biogenic gas migration revealed by seep carbonate paragenesis, Panoche Hills, California. *AAPG Bulletin*, *101*(8), 1309–1340. https://doi.org/10.1306/10171616021

Bonaglia, S. (2015). *Control factors of the marine nitrogen cycle: The role of meiofauna, macrofauna, oxygen and aggregates*. http://urn.kb.se/resolve?urn=urn:nbn:se:su:diva-115036

Bowles, M., & Joye, S. (2011). High rates of denitrification and nitrate removal in cold seep sediments. *The ISME Journal*, *5*(3), 565–567. https://doi.org/10.1038/ismej.2010.134

Bowles, M. W., Mogollón, J. M., Kasten, S., Zabel, M., & Hinrichs, K.-U. (2014). Global rates of marine sulfate reduction and implications for sub–sea-floor metabolic activities. *Science*, *344*(6186), 889–891. https://doi.org/10.1126/science.1249213

Brimblecombe, P. (2014). 10.14—The Global Sulfur Cycle. In H. D. Holland & K. K. Turekian (Eds.), *Treatise on Geochemistry (Second Edition)* (pp. 559–591). Elsevier. https://doi.org/10.1016/B978-0-08-095975-7.00814-7

Brinkmann, T., Specht, C., & Frimmel, F. (2002). Non-linear calibration functions in ion chromatography with suppressed conductivity detection using hydroxide eluents. *Journal of Chromatography. A*, *957*, 99–109. https://doi.org/10.1016/S0021-9673(02)00308-4

Brunnegård, J., Grandel, S., Ståhl, H., Tengberg, A., & Hall, P. O. J. (2004). Nitrogen cycling in deep-sea sediments of the Porcupine Abyssal Plain, NE Atlantic. *Progress in Oceanography*, *63*(4), 159–181. https://doi.org/10.1016/j.pocean.2004.09.004

Büttner, J., Borth, R., Boutwell, J. H., Broughton, P. M. G., & Bowyer, R. C. (1977). Provisional recommendation on quality control in clinical chemistry: Part 6. Quality requirements from the point of view of health care. *Clinica Chimica Acta*, *74*(2), F1–F9. https://doi.org/10.1016/0009-8981(77)90223-6

Callbeck, C. M., Canfield, D. E., Kuypers, M. M. M., Yilmaz, P., Lavik, G., Thamdrup, B., Schubert, C. J., & Bristow, L. A. (2021). Sulfur cycling in oceanic oxygen minimum zones. *Limnology and Oceanography*, *66*(6), 2360–2392. https://doi.org/10.1002/lno.11759

Carlson, C. A., Bates, N. R., Hansell, D. A., & Steinberg, D. K. (2001). Carbon Cycle. In J. H. Steele (Ed.), *Encyclopedia of Ocean Sciences* (pp. 390–400). Academic Press. https://doi.org/10.1006/rwos.2001.0272

Carr, M.-E. (2001). Estimation of potential productivity in Eastern Boundary Currents using remote sensing. *Deep Sea Research Part II: Topical Studies in Oceanography*, *49*(1), 59–80. https://doi.org/10.1016/S0967-0645(01)00094-7

Christensen, J. P., & Rowe, G. T. (1984). Nitrification and oxygen consumption in northwest Atlantic deep-sea sediments. *Journal of Marine Research*, *42*(4), 1099–1116. https://doi.org/10.1357/002224084788520828

Codispoti, L. A., Brandes, J. A., Christensen, J. P., Devol, A. H., Naqvi, S. W. A., Paerl, H. W., & Yoshinari, T. (2001). The oceanic fixed nitrogen and nitrous oxide budgets: Moving

targets as we enter the anthropocene? *Scientia Marina*, *65*(S2), 85–105. https://doi.org/10.3989/scimar.2001.65s285

Cranston, R. E. (1994). Marine sediments as a source of atmospheric methane. *Bulletin of the Geological Society of Denmark, Vol. 41/1*, 101–109.

Dale, A. W., Aguilera, D. R., Regnier, P., Fossing, H., Knab, N. J., & Jørgensen, B. B. (2008). Seasonal dynamics of the depth and rate of anaerobic oxidation of methane in Aarhus Bay (Denmark) sediments. *Journal of Marine Research*, *66*(1), 127–155. https://doi.org/10.1357/002224008784815775

Di Bonito, M., Breward, N., Crout, N., Smith, B., Young, S. D., & Zhang, H. (2018). Chapter 10—Extraction and Characterization of Pore Water in Contaminated Soils. In B. De Vivo, H. E. Belkin, & A. Lima (Eds.), *Environmental Geochemistry (Second Edition)* (pp. 195–235). Elsevier. https://doi.org/10.1016/B978-0-444-63763-5.00011-2

Dong, X., Rattray, J., Campbell, D., Webb, J., Chakraborty, A., Adebayo, O., Matthews, S., Li, C., Fowler, M., Morrison, N., Macdonald, A., Groves, R., Lewis, I., Wang, S., Mayumi, D., Greening, C., & Hubert, C. (2020). Thermogenic hydrocarbon biodegradation by diverse depth-stratified microbial populations at a Scotian Basin cold seep. *Nature Communications*, *11*, 5825. https://doi.org/10.1038/s41467-020-19648-2

Edwards, B. R., Bidle, K. D., & Van Mooy, B. A. S. (2015). Dose-dependent regulation of microbial activity on sinking particles by polyunsaturated aldehydes: Implications for the carbon cycle. *Proceedings of the National Academy of Sciences*, *112*(19), 5909–5914. https://doi.org/10.1073/pnas.1422664112

Engström, P., Dalsgaard, T., Hulth, S., & Aller, R. C. (2005). Anaerobic ammonium oxidation by nitrite (anammox): Implications for N2 production in coastal marine sediments.

Geochimica et Cosmochimica Acta, *69*(8), 2057–2065. https://doi.org/10.1016/j.gca.2004.09.032

Fernandez, C., Farías, L., & Ulloa, O. (2011). Nitrogen Fixation in Denitrified Marine Waters. *PLOS ONE*, *6*(6), e20539. https://doi.org/10.1371/journal.pone.0020539

Fowler, M. (2016). *Petroleum Systems of the Scotian Basin*. *#10871*, 33.

Gámiz-Gracia, L., García-Campaña, A. M., Barrero, F., & Cuadros-Rodríguez, L. (2003). Determination of albumin in biological fluids by flow injection analysis using the peroxyoxalate chemiluminescent system in micellar medium. *Analytical and Bioanalytical Chemistry*, *377*, 281–286. https://doi.org/10.1007/s00216-003-1958-2

Gašparović, B., Penezić, A., Lampitt, R. S., Sudasinghe, N., & Schaub, T. (2018). Phospholipids as a component of the oceanic phosphorus cycle. *Marine Chemistry*, *205*, 70–80. https://doi.org/10.1016/j.marchem.2018.08.002

GIBLIN, A. E., TOBIAS, C. R., SONG, B., WESTON, N., BANTA, G. T., & H.RIVERA-MONROY, V. (2013). The Importance of Dissimilatory Nitrate Reduction to Ammonium (DNRA) in the Nitrogen Cycle of Coastal Ecosystems. *Oceanography*, *26*(3), 124–131.

Gieskes, J., Mahn, C., Day, S., Martin, J. B., Greinert, J., Rathburn, T., & McAdoo, B. (2005). A study of the chemistry of pore fluids and authigenic carbonates in methane seep environments: Kodiak Trench, Hydrate Ridge, Monterey Bay, and Eel River Basin. *Chemical Geology*, *220*(3), 329–345. https://doi.org/10.1016/j.chemgeo.2005.04.002

Government of Canada, F. and O. C. (2018, May 23). *The Scotian shelf: An atlas of human activities*. https://www.dfo-mpo.gc.ca/oceans/publications/scotian-atlas-ecossais/page02-eng.html

Grant, J., Hatcher, A., Macpherson, P., & Schofield, B. (1998). SULFATE REDUCTION AND TOTAL BENTHIC METABOLISM IN SHELF AND SLOPE SEDIMENTS OFF NOVA SCOTIA. *Life & Environment- Laboratoire Arago*, 259–269.

Gruber, N., & Sarmiento, J. L. (1997). Global patterns of marine nitrogen fixation and denitrification. *Global Biogeochemical Cycles*, *11*(2), 235–266. https://doi.org/10.1029/97GB00077

Haddad, P. R. (2000). CHROMATOGRAPHY: LIQUID | Mechanisms: Ion Chromatography. In I. D. Wilson (Ed.), *Encyclopedia of Separation Science* (pp. 696–705). Academic Press. https://doi.org/10.1016/B0-12-226770-2/00321-5

Hammond, D. (2001). Pore Water Chemistry. In J. H. Steele (Ed.), *Encyclopedia of Ocean Sciences* (pp. 2263–2271). Academic Press. https://doi.org/10.1006/rwos.2001.0181

Han, X., Suess, E., Sahling, H., & Wallmann, K. (2004). Fluid venting activity on the Costa Rica margin: New results from authigenic carbonates. *International Journal of Earth Sciences*, *93*(4), 596–611. https://doi.org/10.1007/s00531-004-0402-y

Harris, P. T., & Baker, E. (Eds.). (2020). Hydrocarbon Seep. In *Seafloor Geomorphology as Benthic Habitat (Second Edition)* (pp. i–iii). Elsevier. https://doi.org/10.1016/B978-0-12-814960-7.00061-0

Hasegawa, K., Minakata, K., Suzuki, M., & Suzuki, O. (2021). The standard addition method and its validation in forensic toxicology. *Forensic Toxicology*, *39*(2), 311–333. https://doi.org/10.1007/s11419-021-00585-8

Hedges, J. I. (1992). Global biogeochemical cycles: Progress and problems. *Marine Chemistry*, *39*(1), 67–93. https://doi.org/10.1016/0304-4203(92)90096-S

Herbert, R. A. (1999). Nitrogen cycling in coastal marine ecosystems. *FEMS Microbiology Reviews*, *23*(5), 563–590. https://doi.org/10.1111/j.1574-6976.1999.tb00414.x

Hines, M. E., Bazylinski, D. A., Tugel, J. B., & Berry Lyons, W. (1991). Anaerobic microbial biogeochemistry in sediments from two Basins in the Gulf of Maine: Evidence for iron and manganese reduction. *Estuarine, Coastal and Shelf Science*, *32*(4), 313–324. https://doi.org/10.1016/0272-7714(91)90046-E

Hoehler, T. M., Alperin, M. J., Albert, D. B., & Martens, C. S. (1994). Field and laboratory studies of methane oxidation in an anoxic marine sediment: Evidence for a methanogen-sulfate reducer consortium. *Global Biogeochemical Cycles*, *8*(4), 451–463. https://doi.org/10.1029/94GB01800

Hoehler, T. M., Alperin, M. J., Albert, D. B., & Martens, C. S. (2001). Apparent minimum free energy requirements for methanogenic Archaea and sulfate-reducing bacteria in an anoxic marine sediment. *FEMS Microbiology Ecology*, *38*(1), 33–41. https://doi.org/10.1111/j.1574-6941.2001.tb00879.x

Jilbert, T. (2016). Understanding mud: The importance of sediment biogeochemistry. *Geologi: Magazine of the Geological Society of Finland*, *2016*, 80–87.

Jørgensen, B. B. (1982). Mineralization of organic matter in the sea bed—The role of sulphate reduction. *Nature*, *296*(5858), 643–645. https://doi.org/10.1038/296643a0

Jørgensen, B. B. (2021). Sulfur Biogeochemical Cycle of Marine Sediments. *Geochemical Perspectives*, 145–307. https://doi.org/10.7185/geochempersp.10.2

Jørgensen, B. B., Findlay, A. J., & Pellerin, A. (2019). The Biogeochemical Sulfur Cycle of Marine Sediments. *Frontiers in Microbiology*, *10*, 849. https://doi.org/10.3389/fmicb.2019.00849

Jørgensen, B. B., & Kasten, S. (2006). Sulfur Cycling and Methane Oxidation. In H. D. Schulz & M. Zabel (Eds.), *Marine Geochemistry* (pp. 271–309). Springer-Verlag. https://doi.org/10.1007/3-540-32144-6_8

Joye, S. B., & Anderson, I. C. (2008). Chapter 19—Nitrogen Cycling in Coastal Sediments. In D. G. Capone, D. A. Bronk, M. R. Mulholland, & E. J. Carpenter (Eds.), *Nitrogen in the Marine Environment (Second Edition)* (pp. 867–915). Academic Press. https://doi.org/10.1016/B978-0-12-372522-6.00019-0

Joye, S. B., Boetius, A., Orcutt, B. N., Montoya, J. P., Schulz, H. N., Erickson, M. J., & Lugo, S. K. (2004). The anaerobic oxidation of methane and sulfate reduction in sediments from Gulf of Mexico cold seeps. *Chemical Geology*, *205*(3–4), 219–238. https://doi.org/10.1016/j.chemgeo.2003.12.019

Joye, S. B., Bowles, M. W., Samarkin, V. A., Hunter, K. S., & Niemann, H. (2010). Biogeochemical signatures and microbial activity of different cold-seep habitats along the Gulf of Mexico deep slope. *Deep Sea Research Part II: Topical Studies in Oceanography*, *57*(21), 1990–2001. https://doi.org/10.1016/j.dsr2.2010.06.001

Karaca, D., Hensen, C., & Wallmann, K. (2010). Controls on authigenic carbonate precipitation at cold seeps along the convergent margin off Costa Rica. *Geochemistry, Geophysics, Geosystems*, *11*(8). https://doi.org/10.1029/2010GC003062

Keil, R. (2017). Anthropogenic Forcing of Carbonate and Organic Carbon Preservation in Marine Sediments. *Annual Review of Marine Science*, *9*(1), 151–172. https://doi.org/10.1146/annurev-marine-010816-060724

Kennicutt, M. C., Brooks, J. M., & Denoux, G. J. (1988). Leakage of deep, reservoired petroleum to the near surface on the gulf of Mexico Continental slope. *Marine Chemistry*, *24*(1), 39–59. https://doi.org/10.1016/0304-4203(88)90005-9

Lin, S., & Morse, J. W. (1991). Sulfate reduction and iron sulfide mineral formation in Gulf of Mexico anoxic sediments. *American Journal of Science*, *291*(1), 55–89. https://doi.org/10.2475/ajs.291.1.55

Milucka, J., Ferdelman, T. G., Polerecky, L., Franzke, D., Wegener, G., Schmid, M., Lieberwirth, I., Wagner, M., Widdel, F., & Kuypers, M. M. M. (2012). Zero-valent sulphur is a key intermediate in marine methane oxidation. *Nature*, *491*(7425), 541–546. https://doi.org/10.1038/nature11656

Morse, J. W., & Mackenzie, F. T. (1990). *Geochemistry of Sedimentary Carbonates*. Elsevier.

Mosher, D., & Wach, G. D. (2009). *"Passive" Margin Sedimentation and Reservoir Distribution Along the Scotian Margin*. 8.

Musat, F., Harder, J., & Widdel, F. (2006). Study of nitrogen fixation in microbial communities of oil-contaminated marine sediment microcosms. *Environmental Microbiology*, *8*(10), 1834–1843. https://doi.org/10.1111/j.1462-2920.2006.01069.x

Naehr, T. H., Eichhubl, P., Orphan, V. J., Hovland, M., Paull, C. K., Ussler, W., Lorenson, T. D., & Greene, H. G. (2007). Authigenic carbonate formation at hydrocarbon seeps in continental margin sediments: A comparative study. *Deep Sea Research Part II: Topical Studies in Oceanography*, *54*(11), 1268–1291. https://doi.org/10.1016/j.dsr2.2007.04.010

Nesterenko, P. N., & Paull, B. (2017). Chapter 9—Ion chromatography. In S. Fanali, P. R. Haddad, C. F. Poole, & M.-L. Riekkola (Eds.), *Liquid Chromatography (Second Edition)* (pp. 205–244). Elsevier. https://doi.org/10.1016/B978-0-12-805393-5.00009-9

Oceans: The Largest Active Carbon Reservoir - Science for Humanity - Academic Stories. (n.d.). Retrieved April 4, 2022, from https://academicstories.com/story/science-for-humanity/oceans-the-largest-active-carbon-reservoir

Orcutt, B. N., Joye, S. B., Kleindienst, S., Knittel, K., Ramette, A., Reitz, A., Samarkin, V., Treude, T., & Boetius, A. (2010). Impact of natural oil and higher hydrocarbons on microbial diversity, distribution, and activity in Gulf of Mexico cold-seep sediments. *Deep Sea Research Part II: Topical Studies in Oceanography*, *57*(21), 2008–2021. https://doi.org/10.1016/j.dsr2.2010.05.014

Pastore, P., Favaro, G., Badocco, D., Tapparo, A., Cavalli, S., & Saccani, G. (2005). Determination of biogenic amines in chocolate by ion chromatographic separation and pulsed integrated amperometric detection with implemented wave-form at Au disposable electrode. *Journal of Chromatography A*, *1098*(1), 111–115. https://doi.org/10.1016/j.chroma.2005.08.065

Paull, C. K., Hecker, B., Commeau, R., Freeman-Lynde, R. P., Neumann, C., Corso, W. P., Golubic, S., Hook, J. E., Sikes, E., & Curray, J. (1984). Biological Communities at the Florida Escarpment Resemble Hydrothermal Vent Taxa. *Science*, *226*(4677), 965–967. https://doi.org/10.1126/science.226.4677.965

Peckmann, J., Reimer, A., Luth, U., Luth, C., Hansen, B. T., Heinicke, C., Hoefs, J., & Reitner, J. (2001). Methane-derived carbonates and authigenic pyrite from the northwestern Black Sea. *Marine Geology*, *177*(1), 129–150. https://doi.org/10.1016/S0025-3227(01)00128-1

Peckmann, J., & Thiel, V. (2004). Carbon cycling at ancient methane–seeps. *Chemical Geology*, *205*(3), 443–467. https://doi.org/10.1016/j.chemgeo.2003.12.025

Piper, D., & Campbell, D. (2002). *Surficial geology of the Scotian Slope, eastern Canada*.

Pohl, C. (2005). Ion Chromatography—An overview | ScienceDirect Topics. In *Encyclopedia of Analytical Science-2019* (Third). Science Direct. https://www.sciencedirect.com/topics/chemistry/ion-chromatography

Qian, G., Wang, J., Kan, J., Zhang, X., Xia, Z., Zhang, X., Miao, Y., & Sun, J. (2018). Diversity and distribution of anammox bacteria in water column and sediments of the Eastern Indian Ocean. *International Biodeterioration & Biodegradation*, *133*, 52–62. https://doi.org/10.1016/j.ibiod.2018.05.015

Rickard, D. (2012). Chapter 14—Sedimentary Sulfides. In D. Rickard (Ed.), *Developments in Sedimentology* (Vol. 65, pp. 543–604). Elsevier. https://doi.org/10.1016/B978-0-444-52989-3.00014-3

Riebeek, H. (2011, June 16). *The Carbon Cycle* [Text.Article]. NASA Earth Observatory. https://earthobservatory.nasa.gov/features/CarbonCycle/page1.php

Roberts, H. H. (2001). Fluid and Gas Expulsion on the Northern Gulf of Mexico Continental Slope: Mud-Prone to Mineral-Prone Responses. In *Natural Gas Hydrates: Occurrence, Distribution, and Detection* (pp. 145–161). American Geophysical Union (AGU). https://doi.org/10.1029/GM124p0145

Rodríguez, L. C., Campaña, A. M. G., Barrero, F. A., Linares, C. J., & Ceba, M. R. (1995). Validation of an Analytical Instrumental Method by Standard Addition Methodology. *Journal of AOAC INTERNATIONAL*, *78*(2), 471–476. https://doi.org/10.1093/jaoac/78.2.471

Rohrer, J. S. (2019). Chapter 5—Monitoring Water Contaminants With Ion Chromatography. In S. Ahuja (Ed.), *Advances in Water Purification Techniques* (pp. 115–134). Elsevier. https://doi.org/10.1016/B978-0-12-814790-0.00005-3

Ruff, S. E. (2020). *Microbial Communities and Metabolisms at Hydrocarbon Seeps* (pp. 1–19). https://doi.org/10.1007/978-3-030-34827-4_1

Saxberg, B. E. H., & Kowalski, B. R. (1979). Generalized standard addition method. *Analytical Chemistry*, *51*(7), 1031–1038. https://doi.org/10.1021/ac50043a059

Schulz, H. D. (2006). Quantification of Early Diagenesis: Dissolved Constituents in Pore Water and Signals in the Solid Phase. In H. D. Schulz & M. Zabel (Eds.), *Marine Geochemistry* (pp. 73–124). Springer. https://doi.org/10.1007/3-540-32144-6_3

Smith, S. V., & Mackenzie, F. T. (1987). The ocean as a net heterotrophic system: Implications From the carbon biogeochemical cycle. *Global Biogeochemical Cycles*, *1*(3), 187–198. https://doi.org/10.1029/GB001i003p00187

Sun, X., Higgins, J., & Turchyn, A. V. (2016). Diffusive cation fluxes in deep-sea sediments and insight into the global geochemical cycles of calcium, magnesium, sodium and potassium. *Marine Geology*, *373*, 64–77. https://doi.org/10.1016/j.margeo.2015.12.011

Tajika, E. (1999). Carbon cycle and climate change during the Cretaceous inferred from a biogeochemical carbon cycle model. *Island Arc*, *8*(2), 293–303. https://doi.org/10.1046/j.1440-1738.1999.00238.x

Tarpgaard, I. H., Røy, H., & Jørgensen, B. B. (2011). Concurrent low- and high-affinity sulfate reduction kinetics in marine sediment. *Geochimica et Cosmochimica Acta*, *75*(11), 2997–3010. https://doi.org/10.1016/j.gca.2011.03.028

Treude, T., Krause, S., Maltby, J., Dale, A. W., Coffin, R., & Hamdan, L. J. (2014). Sulfate reduction and methane oxidation activity below the sulfate-methane transition zone in Alaskan Beaufort Sea continental margin sediments: Implications for deep sulfur cycling.

Geochimica et Cosmochimica Acta, *144*, 217–237. https://doi.org/10.1016/j.gca.2014.08.018

Ulloa, O., Canfield, D. E., DeLong, E. F., Letelier, R. M., & Stewart, F. J. (2012). Microbial oceanography of anoxic oxygen minimum zones. *Proceedings of the National Academy of Sciences*, *109*(40), 15996–16003. https://doi.org/10.1073/pnas.1205009109

Valentine, D. L. (2002). Biogeochemistry and microbial ecology of methane oxidation in anoxic environments: A review. *Antonie van Leeuwenhoek*, *81*(1), 271–282. https://doi.org/10.1023/A:1020587206351

van de Velde, S. J., Reinhard, C. T., Ridgwell, A., & Meysman, F. J. R. (2020). Bistability in the redox chemistry of sediments and oceans. *Proceedings of the National Academy of Sciences*, *117*(52), 33043–33050. https://doi.org/10.1073/pnas.2008235117

Vanderborght, J.-P., & Billen, G. (1975). Vertical distribution of nitrate concentration in interstitial water of marine sediments with nitrification and denitrification. *Limnology and Oceanography*, *20*(6), 953–961. https://doi.org/10.4319/lo.1975.20.6.0953

Wang, P., Li, Q., & Li, C.-F. (2014). Chapter 7—Hydrocarbon and Mineral Resources. In P. Wang, Q. Li, & C.-F. Li (Eds.), *Developments in Marine Geology* (Vol. 6, pp. 571–641). Elsevier. https://doi.org/10.1016/B978-0-444-59388-7.00007-X

Wasmund, K., Mußmann, M., & Loy, A. (2017). The life sulfuric: Microbial ecology of sulfur cycling in marine sediments: Microbial sulfur cycling in marine sediments. *Environmental Microbiology Reports*, *9*(4), 323–344. https://doi.org/10.1111/1758-2229.12538

Welsink, H. J., Dwyer, J. D., & Knight, R. J. (1989). *Tectono-Stratigraphy of the Passive Margin Off Nova Scotia*. https://doi.org/10.1306/M46497C14

Widdel, F., & Rabus, R. (2001). Anaerobic biodegradation of saturated and aromatic hydrocarbons. *Current Opinion in Biotechnology*, *12*(3), 259–276. https://doi.org/10.1016/S0958-1669(00)00209-3

Yang, Y., Chen, Q., & Zhang, G. (n.d.). *DETERMINATION OF SULFATE IN COASTAL SALT MARSH SEDIMENTS WITH HIGH-CHLORIDE CONCENTRATION BY ION CHR*. 11.

Zehr, J. P., & Capone, D. G. (1996). Problems and promises of assaying the genetic potential for nitrogen fixation in the marine environment. *Microbial Ecology*, *32*(3). https://doi.org/10.1007/BF00183062

Zellmer, D. L. (1998, September 2). *Standard Addition*. Standard Addition. http://zimmer.csufresno.edu/~davidz/Chem106/StdAddn/StdAddn.html

Zenkevich, I., & Klimova, I. (2006). Use of the standard addition method in quantitative chromatographic analysis. *Journal of Analytical Chemistry*, *61*, 967–972. https://doi.org/10.1134/S1061934806100042